INTERNATIONAL JOURNAL FOR NUMERICAL METHODS IN FLUIDS
Int. J. Numer. Meth. Fluids 2008; **57**:47–92
Published online 26 September 2007 in Wiley InterScience (www.interscience.wiley.com). DOI: 10.1002/fld.1620

Parameter estimation for a three-dimensional numerical barotropic tidal model with adjoint method

Jicai Zhang and Xianqing Lu*, †

Laboratory of Physical Oceanography, Ocean University of China, Qingdao 266003, China

SUMMARY

The parameters of a three-dimensional (3-D) barotropic tidal model are estimated using the adjoint method. The mode splitting technique is employed in both forward and adjoint models. In the external mode, the alternating direction implicit method is used to discretize the two-dimensional depth-averaged equations and a semi-implicit scheme is used for the 3-D internal mode computations. In this model the bottom friction is expressed in terms of bottom velocity which is different from the previous works. Besides, the bottom friction coefficients (BFCs) are supposed to be spatially varying, i.e. the BFC at some grid points are selected as the independent BFC, while the BFC at the other grid points can be obtained through linear interpolation with these independent BFCs. On the basis of the simulation of M_2 tide in the Bohai and North Yellow Seas (BNYS), twin experiments are carried out to invert the prescribed distributions of model parameters. The parameters inverted are the Fourier coefficients of open boundary conditions (OBCs), the BFC and the vertical eddy viscosity profiles. In these twin experiments, the real topography of BNYS is installed. The 'observations' are produced by the tidal model and recorded at the position of TOPEX/Poseidon altimeter data, tidal gauge data and current data. The experiments discuss the influence of initial guesses, model errors and data number. The inversion has obtained satisfactory results and the prescribed distributions have been successfully inverted. The results indicate that the inversion of BFC is more sensitive to data error than that of OBC and the vertical eddy viscosity profiles. Copyright © 2007 John Wiley & Sons, Ltd.

Received 19 April 2007; Revised 10 August 2007; Accepted 16 August 2007

KEY WORDS: parameter estimation; three dimensional; adjoint method; tidal model

*Correspondence to: Xianqing Lu, Laboratory of Physical Oceanography, Ocean University of China, Qingdao 266003, China.
†E-mail: xqinglv@ouc.edu.cn

Contract/grant sponsor: State Ministry of Science and Technology of China; contract/grant number: 2007AA09Z118
Contract/grant sponsor: National Basic Research Program of China; contract/grant number: 2005CB422308
Contract/grant sponsor: Specialized Research Fund; contract/grant number: 20050423007

Copyright © 2007 John Wiley & Sons, Ltd.

1. INTRODUCTION

Several numerical methods have been widely used in the discretization of time-dependent three-dimensional (3-D) primitive equations. The time integration schemes of these methods can be fully explicit (see, Reference [1]), semi-implicit (e.g. References [2–4]) or fully implicit [5]. For large-scale oceanic problems, the applications of 3-D models are becoming a reality with the aid of modern computers. The fully explicit finite difference method is relatively simple to implement, except that its time step is strictly restricted by the Courant–Friedrich–Lewy (CFL) stability criterion [6]. At present, many existing ocean models are based on an alternating direction implicit (ADI) method. ADI method results in computational efficiency superior to fully explicit methods because their improved stability allows large time steps to be employed. Since the model must simulate both the velocity field and the ocean surface elevation, a technique known as mode splitting (see, Reference [7]) has been used in several ocean models. In the model formulation, the governing system of equations is split into an external mode and an internal mode. A system of two-dimensional (2-D) vertically integrated equations (external mode) is solved independently from the 3-D equations (internal mode). The external mode can calculate the ocean surface elevation efficiently even if a small integration time step is required. The solution of the more computationally intensive 3-D internal mode equations can be achieved by using a large time step. In this paper, a numerical tidal model based on the 3-D primitive equations is established to simulate the barotropic tide in the Bohai Sea and the North Yellow Sea (BNYS). The numerical schemes for solving the equations of motion and continuity use the internal–external mode splitting technique. The ADI method is employed for the external mode computations which give the surface elevations and depth-averaged currents. The time step of external mode is thus not restricted by the CFL condition. A semi-implicit scheme is used for the internal mode computations, which give the vertical structure of the currents. The time step of internal mode can be significantly longer than that of the external mode. As a consequence, the overall computational speed can be several times faster than that of the general explicit models.

Among all the data assimilation methods, four-dimensional variational (4DVAR) data assimilation is one of the most effective and powerful approaches. It is an advanced data assimilation method that involves the adjoint method and has the advantage of directly assimilating various observations distributed in time and space into numerical models while maintaining dynamical and physical consistency with the model. The earlier applications of adjoint assimilation method in oceanography were addressed by Bennett and McIntosh [8] and Prevost and Salmon [9] who applied the weak constraint formalism of Sasaki [10] to a tidal flow problem and a geotrophic flow problem, respectively. Thacker and Long [11] then employed the strong constraint formalism in which the model equations are imposed as exact constraints on the minimization. The adjoint method is a powerful tool for parameter estimation. Panchang and O'Brien [12] estimated the bottom drag coefficient in a tidal channel using some experimental results. The phase speeds were estimated by Smedstad and O'Brien [13] in a reduced gravity model for the tropical Pacific Ocean. The wind stress coefficient and the oceanic eddy viscosity profile were estimated in the work of Yu and O'Brien [14] and the work was extended to optimize the initial condition (see, Reference [15]). Ghil and Malanotte-Rizzoli [16] gave an important comprehensive review, including issues of parameter estimation, about adjoint methodology in meteorology and oceanography. Das and Larder [17, 18] estimated the bottom friction coefficient (BFC) and water depth in a 2-D tidal model. Lardner [19] estimated the open boundary conditions (OBCs) in the same 2-D tidal model.

Copyright © 2007 John Wiley & Sons, Ltd.

DOI: 10.1002/fld

By assimilating the velocity data from one or more current meters, Lardner and Das [20] estimated the eddy viscosity profile in a quasi-3-D numerical tidal and storm surge model. Lardner and Song [21] extended the work to estimate the eddy viscosity profile and friction coefficients. Navon [22] surveyed briefly the state of the art of parameter estimation in meteorology and oceanography in view of applications of 4DVAR data assimilation techniques to inverse parameter estimation problems. Lu and Hsieh [23–25] developed an adjoint model for a simple equatorial ocean model that was coupled to a simple atmospheric model and the parameters in this coupled model were estimated. Marotzke *et al.* [26] constructed the adjoint model of the MITGCM (Massachusetts Institute of Technology ocean general circulation model) using R. Giering's software tool Tangent-linear and Adjoint Model Compiler. More recently, Heemink *et al.* [27] assimilated tide gauge and altimeter data into a 3-D shallow water model to estimate the OBC, the friction and viscosity parameters and water depth. Zhang *et al.* [28, 29] estimated the wind drag coefficient and the lateral tidal OBC by assimilating pseudo-observations into a 2-D Princeton Ocean Model (POM). Peng and Xie [30] developed an adjoint model of the 3-D nonlinear POM to construct a 4DVAR algorithm for coastal ocean prediction. Lu and Zhang [31] carried out twin and practical experiments to invert the spatially varying BFC in a 2-D tidal model by assimilating the Topex/Poseidon (T/P) satellite data and tidal gauge data. In this paper, the model described in the first paragraph is taken as the forward model and an adjoint tidal model is constructed. Moreover, the OBC, the BFC and the vertical eddy viscosity profile are inverted by carrying out identical twin experiments.

As noted by Yeh in the work of ground water flow parameter estimation, the inverse or parameter estimation problem is often ill posed and beset by instability and nonuniqueness, particularly if one seeks parameters distributed in space and time domain [32]. The same viewpoint has been put forward in References [13, 17, 18, 20, 27, 33, 34]. In these works they proposed to insert an additional criterion into the cost function named the penalty term, and by doing this, large fluctuations will be penalized to ensure the parameters varying smoothly. According to the viewpoint of Smedstad and O'Brien, adding prior information about the parameters (penalty term) increases the chance that the cost function will be convex (namely, the solution to the inverse problem is unique) [13]. Lardner and Das pointed out that this term is useful especially when the data contain observation error [20]. In this paper we take two measures to overcome this difficulty. First, the minimization algorithm used in Lu and Zhang [31] is employed to ensure that the cost function can decrease continuously without large fluctuations. Second, the dimension of the parameter space is reduced. In the present study, the BFC at some grid points is selected as the independent BFC, while the BFCs at the other grid points can be obtained through linear interpolation with these independent BFCs (see, Reference [31]). In the previous works on the 3-D adjoint tidal model (e.g. References [20, 21]), the bottom friction is expressed in terms of depth-averaged velocities, and the horizontal shear stresses and the convective terms are neglected in the momentum equations. However, for the bottom friction effect, turbulent boundary layer models of the near-bottom flow indicate that it is physically realistic to use a quadratic dependence of bottom friction on the bottom velocity. In our model the bottom friction is expressed in terms of bottom velocity while the horizontal shear stresses and the convective terms are included.

The paper is organized as follows. The numerical 3-D tidal model is presented in Section 2. The adjoint model is shown in Section 3. In Section 4, identical twin experiments are carried out to invert the prescribed parameter distributions and the results are analyzed. Finally, Section 5 provides main conclusions and discussions of some related issues of this study.

Copyright © 2007 John Wiley & Sons, Ltd.

DOI: 10.1002/fld

2. NUMERICAL TIDAL MODEL (FORWARD MODEL)

2.1. Governing equations

Assuming the pressure is hydrostatic and the density is constant, the 3-D, nonlinear, time-dependent, free-surface, primitive equations of motion and continuity on spherical coordinates are given as follows:

$$\frac{\partial u}{\partial t}+\frac{u}{a}\frac{\partial u}{\partial \lambda}+\frac{v}{R}\frac{\partial u}{\partial \phi}+w\frac{\partial u}{\partial z}-\frac{uv\tan\phi}{R}-fv+\frac{g}{a}\frac{\partial \zeta}{\partial \lambda}-A_h\Delta u-\frac{\partial}{\partial z}\left(A_v\frac{\partial u}{\partial z}\right) \tag{1}$$

$$\frac{\partial v}{\partial t}+\frac{u}{a}\frac{\partial v}{\partial \lambda}+\frac{v}{R}\frac{\partial v}{\partial \phi}+w\frac{\partial v}{\partial z}+\frac{u^2\tan\phi}{R}+fu+\frac{g}{R}\frac{\partial \zeta}{\partial \phi}-A_h\Delta v-\frac{\partial}{\partial z}\left(A_v\frac{\partial v}{\partial z}\right)=0 \tag{2}$$

$$\frac{\partial w}{\partial z}+\frac{1}{a}\frac{\partial u}{\partial \lambda}+\frac{1}{a}\frac{\partial (v\cos\phi)}{\partial \phi}=0 \tag{3}$$

where t is the time, λ and ϕ are the east longitude and north latitude, respectively, ζ is the sea surface elevation above the undisturbed sea level, $u(x, y, z, t)$, $v(x, y, z, t)$ and $w(x, y, z, t)$ are the velocity components in the horizontal x-, y-direction and in the vertical z-direction, respectively, R is the radius of the Earth, $a=R\cos\phi$, f is the Coriolis parameter and $f=2\Omega\sin\phi$, where Ω represents the angular speed of Earth's rotation, g is the acceleration due to gravity, A_h and A_v are the coefficients of horizontal and vertical eddy viscosity, respectively, Δ is the Laplace operator and $\Delta(u, v)=a^{-1}[a^{-1}\partial_\lambda(\partial_\lambda(u, v))+R^{-1}\partial_\phi(\cos\phi\partial_\phi(u, v))]$.

The kinematic boundary condition at the moving free surface and at the impermeable bottom and the dynamic boundary condition at the bottom are given by (4), (5) and (6), respectively,

$$\frac{\partial \zeta}{\partial t}+\frac{u}{a}\frac{\partial \zeta}{\partial \lambda}+\frac{v}{R}\frac{\partial \zeta}{\partial \phi}=-w \tag{4}$$

$$\frac{u}{a}\frac{\partial h}{\partial \lambda}+\frac{v}{R}\frac{\partial h}{\partial \phi}=w \tag{5}$$

$$A_v\frac{\partial}{\partial z}(u, v)=C_d(u_b^2+v_b^2)^{1/2}(u_b, v_b) \tag{6}$$

where C_d is the BFC, h is the undisturbed water depth and (u_b, v_b) is the velocity vector at the sea bed.

Integrating Equations (1)–(3) from the sea bed $z=h$ to the free surface $z=-\zeta$ and applying the boundary conditions (4)–(6), we can get the 2-D vertically averaged equations as follows:

$$\frac{\partial \zeta}{\partial t}=-\frac{1}{a}\left[\frac{\partial (HU)}{\partial \lambda}+\frac{\partial (HV\cos\phi)}{\partial \phi}\right] \tag{7}$$

$$\frac{\partial U}{\partial t}=-\frac{g}{a}\frac{\partial \zeta}{\partial \lambda}+fV+A_h\Delta U-(L_x+R_x) \tag{8}$$

$$\frac{\partial V}{\partial t}=-\frac{g}{R}\frac{\partial \zeta}{\partial \phi}-fU+A_h\Delta V-(L_y+R_y) \tag{9}$$

Copyright © 2007 John Wiley & Sons, Ltd.

DOI: 10.1002/fld

where $U(x, y, t)$ and $V(x, y, t)$ are the depth-averaged horizontal velocities, L_x, L_y and R_x, R_y are the convective terms and bottom friction terms, respectively.

2.2. Discretization of model equations

Arakawa C grid is used in the finite difference forms (see, Reference [35]) and the free-surface elevation is defined in the center of the cell, while the velocity components are located at the faces. As shown in Figure 1, each cell is numbered at its center with indices (i, j, k). The u-velocity is defined at half-integer i and integers j and k; v-velocity is defined at integers i and k and half-integer j; w-velocity is then defined at integers i and j and half-integer k; the free-surface elevation ζ and undisturbed water depth h are defined at integers i and j. The undisturbed water depth h is specified at the u and v horizontal points: $hu_{i+1/2,j} = (h_{i,j} + h_{i+1,j})/2$, $hv_{i,j+1/2} = (h_{i,j} + h_{i,j+1})/2$. We suppose that the water is divided into M layers and the thickness of each layer is defined to be $\Delta_l, (l = 1, 2, \ldots, M)$. In detail, M is the function of horizontal coordinates, i.e. $M = M_{i,j} \cdot \Delta z_{i+1/2,j,k}$ and $\Delta z_{i,j+1/2,k}$ are defined to be the thickness of the kth water layer at u and v points, respectively. Because of the irregular bottom and the moving free surface, the surface layers and the bottom layers are usually not fully filled and the thickness of these layers is defined to be the wetted height of the corresponding face. Therefore, the thickness of the surface layer will change with the time level. In addition, the number of layers is specified at the u and v horizontal points. At u points the number of layers is Kx and $Kx_{i+1/2,j} = \min(M_{i,j}, M_{i+1,j})$; at v points it is Ky and $Ky_{i,j+1/2} = \min(M_{i,j}, M_{i,j+1})$. The time-dependent total water depth is given by $H_{i,j} = h_{i,j} + \zeta_{i,j}$.

In this model, the mode splitting technique is employed. Equations (1)–(3) and (7)–(9) are taken as the governing equations of internal mode and external mode, respectively. The external mode can calculate the ocean surface elevation efficiently even if a small integration time step is required. The solution of the more computationally intensive 3-D internal mode equations can be achieved by using a large time step. The time step of internal mode ΔT is assumed to be q times longer than that of external mode, i.e. $\Delta T = q\Delta t$, where q is even and Δt is the time step of the external mode. The L_x, L_y and R_x, R_y in Equations (8)–(9) are the convective terms and bottom friction terms, respectively, which are computed in the internal mode. The coupling relation between

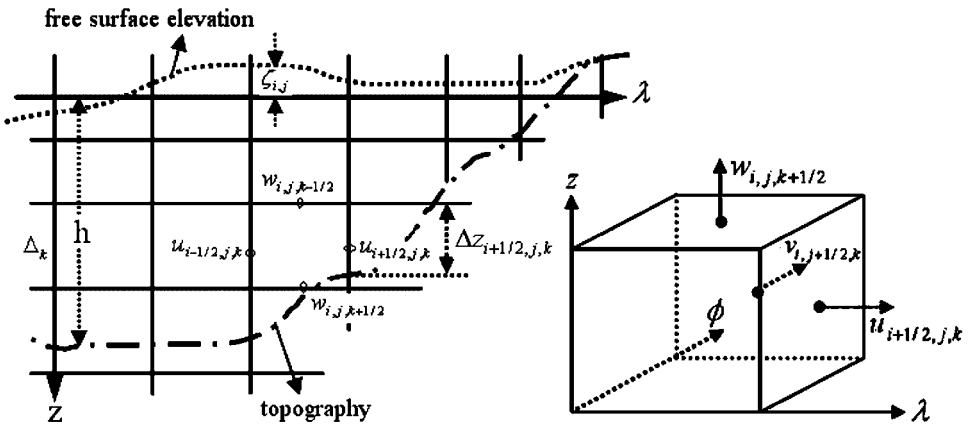

Figure 1. Layout of the computational grids and cells.

Copyright © 2007 John Wiley & Sons, Ltd.

DOI: 10.1002/fld

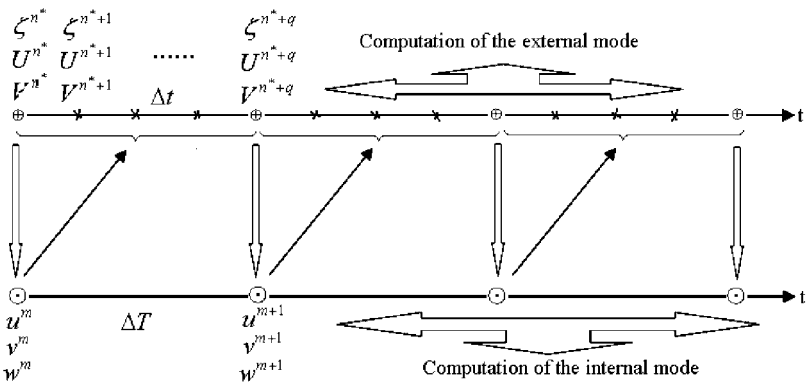

Figure 2. The coupling relation between the external and the internal mode computations; q is even and equals to four in the figure for instance; $n^* = q \times m$, where n^* and m are the time index of external mode and internal mode, respectively. The free-surface elevation calculated in the external mode at $\oplus$ is used in the computation of internal mode and the u, v, w calculated in the internal mode at $\odot$ are used to compute Lx, Ly, Rx and Ry in Equations (8)–(9), i.e. the convective terms and bottom friction terms of external mode.

the internal mode and the external mode is shown in Figure 2. The discretization of external mode and internal mode is described in Appendices A.1 and A.2, respectively.

2.3. Boundary conditions

For the external mode, the free-surface elevation of M_2 tide at the jth time step is given as $\zeta^{\mathrm{j}}_{O_l,P_l} = a_{0,l} + [a_l \cos(\omega \mathrm{j}\Delta t) + b_l \sin(\omega \mathrm{j}\Delta t)]$ along the open boundaries, where (O_l, P_l) stands for the grid points at the open boundaries, ω denotes the frequency of M_2 constituent and a_l, b_l are the Fourier coefficients.

For the internal mode, the Orlanski radiation condition is applied. Assuming that φ_b is the velocity of the points at open boundaries, b is the index of these points and m is the index of time step, the Orlanski radiation condition is given by

$$\varphi_b^{m+1} = [\varphi_b^{m-1}(1-\mu) + 2\mu\varphi_{b\mp1}^{m}]/(1+\mu)$$

where

$$\mu = \begin{cases} 1 & \text{if } C_L \geqslant 1 \\ C_L & \text{if } 0 < C_L < 1 \\ 0 & \text{if } C_L \leqslant 0 \end{cases} \quad \text{and} \quad C_L = \frac{\varphi_{b\mp1}^{m-2} - \varphi_{b\mp1}^{m}}{\varphi_{b\mp1}^{m} + \varphi_{b\mp1}^{m-2} - 2\varphi_{b\mp2}^{m-1}}$$

Closed boundary conditions for both the internal and the external mode are zero flow normal to the coast. That is, $\vec{\mathbf{u}} \cdot \vec{\mathbf{n}} = \mathbf{0}$ for the grid points at closed boundary, where $\vec{\mathbf{n}}$ is the outward unit vector and $\vec{\mathbf{u}} = (\mathbf{u}, \mathbf{v})$ is the velocity vector.

Copyright © 2007 John Wiley & Sons, Ltd.

DOI: 10.1002/fld

3. ADJOINT MODEL

3.1. Construction of adjoint model

The adjoint method is a powerful tool for parameter estimation. Thacker and Long [11] first employed the strong constraint formalism in which the model equations were imposed as exact constraints on the minimization. The basic idea of the adjoint method is quite simple: A model is defined by an algorithm and its independent variables such as initial conditions, boundary conditions and empirical parameters. The cost function that measures the data misfit between the model output and observations is minimized through optimizing the independent variables. In detail, the cost function decreases along the opposite direction of the gradients with respect to the control variables, and this gradient is calculated by what has become known as the adjoint model. On the basis of the forward model in Section 2, its adjoint model is constructed in this section.

First, the cost function is defined as

$$\begin{aligned} J(\zeta,u,v)=&\frac{1}{2}\sum_{n=1}^{\text{ite}}\sum_{(i,j)\in D}(\zeta_{i,j}^{n}-\hat{\zeta}_{i,j}^{n})^{\mathrm{T}}K_{\zeta}(\zeta_{i,j}^{n}-\hat{\zeta}_{i,j}^{n})\\ &+\frac{1}{2}\sum_{m=1}^{\text{iti}}\sum_{(i,j,k)\in D}[(u_{i,j,k}^{m}-\hat{u}_{i,j,k}^{m})^{\mathrm{T}}K_{u}(u_{i,j,k}^{m}-\hat{u}_{i,j,k}^{m})\\ &+(v_{i,j,k}^{m}-\hat{v}_{i,j,k}^{m})^{\mathrm{T}}K_{v}(v_{i,j,k}^{m}-\hat{v}_{i,j,k}^{m})] \end{aligned} \tag{10}$$

where n and m are the time index of external mode and internal mode, respectively, D denotes the computing area, $\zeta_{i,j}^{n}$, $u_{i,j,k}^{m}$ and $v_{i,j,k}^{m}$ are the model produced, $\hat{\zeta}_{i,j}^{n}$, $\hat{u}_{i,j,k}^{m}$ and $\hat{v}_{i,j,k}^{m}$ are the observations. Here K_{ζ}, K_u and K_v are the weighting matrixes and theoretically should be the inverse of the observation error covariance matrix. That is, the cost function is weighted more heavily toward the observations that are most accurate or important. However, determining the correct form for K_{ζ}, K_u and K_v is far from easy (see, Reference [36]). In this paper, the numerical experiments are twin ones and the 'observations' are generated by the tidal model; therefore, by assuming that the errors in the data are uncorrelated and equally weighted, K_{ζ}, K_u and K_v are reduced to unit matrixes (e.g. Reference [15]). ite and iti are the number of time steps of external mode and internal mode, respectively, and certainly ite$=q\times$iti.

Then the Lagrangian function is given by

$$\begin{aligned} L=&J(\zeta,u,v)\\ &+\sum_{m=1}^{\text{iti}}\sum_{i,j,k\in D}\left\{\mu_{i+1/2,j,k}^{m}\left[\frac{u_{i+1/2,j,k}^{m}-u_{i+1/2,j,k}^{m-1}}{\Delta T}+lx_{i+1/2,j,k}^{m-1}-f(v_{i,j,k}^{m-1})^{*}+\frac{g}{a_j}\frac{\zeta_{i+1,j}-\zeta_{i,j}}{\Delta\lambda}\right.\right.\\ &\left.\left.-A_h\Delta u_{i+1/2,j,k}^{m-1}-\frac{Av_{i,j,k-1/2}\frac{u_{i+1/2,j,k-1}^{m}-u_{i+1/2,j,k}^{m}}{\Delta z_{i+1/2,j,k-1/2}}-Av_{i,j,k+1/2}\frac{u_{i+1/2,j,k}^{m}-u_{i+1/2,j,k+1}^{m}}{\Delta z_{i+1/2,j,k+1/2}}}{\Delta z_{i+1/2,j,k}}\right]\right\} \end{aligned}$$

Copyright © 2007 John Wiley & Sons, Ltd.

DOI: 10.1002/fld

$$+\sum_{m=1}^{\text{iti}}\sum_{i,j,k\in D}\left\{\gamma_{i,j+1/2,k}^{m}\left[\frac{v_{i,j+1/2,k}^{m}-v_{i,j+1/2,k}^{m-1}}{\Delta T}+ly_{i,j+1/2,k}^{m-1}+f(u_{i,j,k}^{m-1})^{*}+\frac{g}{R}\frac{\zeta_{i,j+1}-\zeta_{i,j}}{\Delta\phi}\right.\right.$$

$$\left.\left.-A_h\Delta v_{i,j+1/2,k}^{m-1}-\frac{Av_{i,j,k-1/2}\frac{v_{i,j+1/2,k-1}^{m}-v_{i,j+1/2,k}^{m}}{\Delta z_{i,j+1/2,k-1/2}}-Av_{i,j,k+1/2}\frac{v_{i,j+1/2,k}^{m}-v_{i,j+1/2,k+1}^{m}}{\Delta z_{i,j+1/2,k+1/2}}}{\Delta z_{i,j+1/2,k}}\right]\right\}$$

$$+\sum_{l=1}^{\text{ite}/2}\sum_{i,j\in D}\left\{\beta_{i,j}^{2l-1}\left[\frac{\zeta_{i,j}^{2l-1}-\zeta_{i,j}^{2l-2}}{\Delta t}+\frac{Hx_{i+1/2,j}^{2l-2}U_{i+1/2,j}^{2l-1}-Hx_{i-1/2,j}^{2l-2}U_{i-1/2,j}^{2l-1}}{a_j\Delta\lambda}\right.\right.$$

$$\left.\left.+\frac{Hy_{i,j+1/2}^{2l-2}V_{i,j+1/2}^{2l-2}\cos\phi_{j+1/2}-Hy_{i,j-1/2}^{2l-2}V_{i,j-1/2}^{2l-2}\cos\phi_{j+1/2}}{a_j\Delta\phi}\right]\right\}$$

$$+\sum_{l=1}^{\text{ite}/2}\sum_{i,j\in D}\left\{\tau_{i+1/2,j}^{2l-1}\left[\frac{U_{i+1/2,j}^{2l-1}-U_{i+1/2,j}^{2l-2}}{\Delta t}+\frac{g(\zeta_{i+1,j}^{2l-1}-\zeta_{i,j}^{2l-1})}{a_j\Delta\lambda}+Lx_{i+1/2,j}\right.\right.$$

$$\left.\left.+Rx_{i+1/2,j}-f(V_{i,j}^{2l-2})^{*}-A_h\Delta U_{i+1/2,j}^{2l-2}\right]\right\}$$

$$+\sum_{l=1}^{\text{ite}/2}\sum_{i,j\in D}\left\{\delta_{i,j+1/2}^{2l-1}\left[\frac{V_{i,j+1/2}^{2l-1}-V_{i,j+1/2}^{2l-2}}{\Delta t}+\frac{g(\zeta_{i,j+1}^{2l-2}-\zeta_{i,j}^{2l-2})}{R\Delta\phi}+Ly_{i,j+1/2}\right.\right.$$

$$\left.\left.+Ry_{i,j+1/2}+f(U_{i,j}^{2l-2})^{*}-A_h\Delta V_{i,j+1/2}^{2l-2}\right]\right\}$$

$$+\sum_{l=1}^{\text{ite}/2}\sum_{i,j\in D}\left\{\beta_{i,j}^{2l-2}\left[\frac{\zeta_{i,j}^{2l-2}-\zeta_{i,j}^{2l-3}}{\Delta t}\right.\right.$$

$$+\frac{Hy_{i,j+1/2}^{2l-3}V_{i,j+1/2}^{2l-2}\cos\phi_{j+1/2}-Hy_{i,j-1/2}^{2l-3}V_{i,j-1/2}^{2l-2}\cos\phi_{j+1/2}}{a_j\Delta\phi}$$

$$\left.\left.+\frac{Hx_{i+1/2,j}^{2l-3}U_{i+1/2,j}^{2l-3}-Hx_{i-1/2,j}^{2l-3}U_{i-1/2,j}^{2l-3}}{a_j\Delta\lambda}\right]\right\}$$

$$+\sum_{l=1}^{\text{ite}/2}\sum_{i,j\in D}\left\{\delta_{i,j+1/2}^{2l-2}\left[\frac{V_{i,j+1/2}^{2l-2}-V_{i,j+1/2}^{2l-3}}{\Delta t}+\frac{g(\zeta_{i,j+1}^{2l-2}-\zeta_{i,j}^{2l-2})}{R\Delta\phi}+Ly_{i,j+1/2}\right.\right.$$

$$\left.\left.+Ry_{i,j+1/2}+f(U_{i,j}^{2l-3})^{*}-A_h\Delta V_{i,j+1/2}^{2l-3}\right]\right\}$$

Copyright © 2007 John Wiley & Sons, Ltd.

DOI: 10.1002/fld

$$+\sum_{l=1}^{\text{ite}/2}\sum_{i,j\in D}\left\{\tau_{i+1/2,j}^{2l-2}\left[\frac{U_{i+1/2,j}^{2l-2}-U_{i+1/2,j}^{2l-3}}{\Delta t}+\frac{g(\zeta_{i+1,j}^{2l-3}-\zeta_{i,j}^{2l-3})}{a_j\Delta\lambda}+Lx_{i+1/2,j}\right.\right.$$

$$\left.\left.+Rx_{i+1/2,j}-f(V_{i,j}^{2l-3})^*-A_h\Delta U_{i+1/2,j}^{2l-3}\right]\right\}$$

where μ, γ, β, τ and δ denote the adjoint variables of u, v, ζ, U and V, respectively. It should be noted that the ADI method in forward model is considered in the construction of Lagrangian function. As a result, there are also external mode and internal mode in the adjoint model. In order to express clearly, the external mode and the internal mode of forward model and the external mode and internal mode of adjoint model will be expressed briefly by FE, FI, AE and AI, respectively. The numerical schemes of adjoint model are given in Appendices B.1 and B.2.

3.2. Optimization of model parameters

In this paper, the parameters that will be optimized are the Fourier coefficients of OBC (a_l and b_l in Section 2.3), BFC (C_d) and vertical eddy viscosity coefficient (A_v). Having determined μ, γ, β, τ, δ in Appendix B, the gradients of cost function with respect to model parameters can thus be calculated.

3.2.1. Optimization of bottom friction coefficient. T/P altimetry has reopened the problem of how tidal dissipation is to be allocated [37]. The bottom friction is closely related to the ocean topography and plays an important role in the tidal phenomenon. For example, tidal dissipation models are usually based on a frictional bottom boundary layer in which the work done by the bottom friction is proportional to the friction coefficient and the velocity cubed (see, Reference [37]). Therefore, it is necessary to depict the bottom friction effect clearly. In tidal models, the bottom friction effect is parametrized by the BFC. So far, the following methods have been employed to deal with the BFC. First, the BFC has been taken as a constant over the whole computing domain (e.g. References [38, 39]). Second, the computing domain is divided into several subdomain and different BFCs are used in different subdomains (e.g. References [40, 41]). Third, the BFCs are assumed to be spatially varying (see, References [27, 31, 34]). The first two methods have been widely used in the tidal simulations, but have relatively low accuracy. The third method can be realized only if the adjoint method is employed. Reasonable simulation results can be obtained by optimizing the spatially varying BFC and the calibration can become an automatic process performed by the computer. However, too many model parameters would then lead to identifiability problem [27], so the number of parameters should be reduced. In this paper, the BFCs at some grid points are chosen as the independent BFCs, while the BFCs at the other grid points can be obtained through linear interpolation with these independent BFCs [31, 34]. In this paper the independent BFCs are selected uniformly over each $1^\circ\times 1^\circ$ area.

Let $b_{ii,jj}$ be a series of independent BFC and $k_{i,j}$ the results of linear interpolation with $b_{ii,jj}$, then we have the following relation:

$$k_{i,j}=\sum_{ii,jj}\phi_{i,j,ii,jj}\times b_{ii,jj}$$

Copyright © 2007 John Wiley & Sons, Ltd.

DOI: 10.1002/fld

where $\phi_{i,j,ii,jj}$ is the coefficient of linear interpolation ($\phi_{i,j,ii,jj}=W_{i,j,ii,jj}/\sum_{ii,jj}W_{i,j,ii,jj}$), $W_{i,j,ii,jj}$ is the weighted coefficient ($W_{i,j,ii,jj}=(R^2-r^2_{i,j,ii,jj})/(R^2+r^2_{i,j,ii,jj})$) of the Cressman form [42], $r_{i,j,ii,jj}$ is the distance from grid point (i,j) to (ii,jj) and R is the influence radius. The gradients of cost function with respect to the independent BFCs are given by $\partial L/\partial b_{ii,jj}=0$ which yields

$$\partial J/\partial b_{ii,jj}+\sum_{n,i,j}\left(\phi_{i+1/2,j,ii,jj}\times\frac{\tau^n_{i+1/2,j}r^{|n/q|+1}_{i+1/2,j,Kx}}{h_{i+1/2,j}+\zeta^n_{i+1/2,j}}\right)+\left(\phi_{i,j+1/2,ii,jj}\times\frac{\delta^n_{i,j+1/2}r^{|n/q|+1}_{i,j+1/2,Ky}}{h_{i,j+1/2}+\zeta^n_{i,j+1/2}}\right)$$
$$\times\sum_{m,i,j}(\phi_{i+1/2,j,ii,jj}\times\mu^m_{i+1/2,j,Kx}r^m_{i+1/2,j,Kx})+(\phi_{i,j+1/2,ii,jj}\times\gamma^m_{i,j+1/2,Ky}r^m_{i,j+1/2,Ky})=0$$

where

$$r^m_{i+1/2,j,Kx}=u^m_{i+1/2,j,Kx}\sqrt{(u^{m-1}_{i+1/2,j,Kx})^2+[(v^{m-1}_{i,j,Kx})^*]^2}$$

and

$$r^m_{i,j+1/2,Ky}=v^m_{i,j+1/2,Ky}\sqrt{(v^{m-1}_{i,j+1/2,Ky})^2+[(u^{m-1}_{i,j,Ky})^*]^2}$$

where n and m are the time index of external mode and internal mode, respectively. Because the cost function decreases along the opposite direction of the gradient, we can obtain the correction of the independent BFC as

$$K_c(b_{ii,jj}-\hat{b}_{ii,jj})+(\partial J/\partial b_{ii,jj})\|\partial J/\partial b\|_2=0$$

i.e.

$$b_{ii,jj}=\hat{b}_{ii,jj}-\frac{1}{K_c}(\partial J/\partial b_{ii,jj})\|\partial J/\partial b\|_2=0$$

where

$$\|\partial J/\partial b\|_2=\left(\sum_{ii,jj}(\partial J/\partial b_{ii,jj})^2\right)^{1/2}$$

$\hat{b}_{ii,jj}$ and $b_{ii,jj}$ are prior and optimized values of independent BFCs, respectively, the coefficient K_c represents the smoothness of BFC in the iterative process. $1/K_c$ is taken as 10^{-4}, i.e. $K_c=10^4$ which is obtained through a trial and error procedure. The more detailed analysis about K_c will be shown in Section 4.3, so will the K_a, K_b in Section 3.2.2 and K_v in Section 3.2.3.

3.2.2. Optimization of open boundary conditions. Among all the parameters in the tidal model, the OBCs are the most important. And a major difficulty faced by numerical models of tidal flow concerns the treatment of open boundaries [19]. Recently, the works on the inversion of OBC using the adjoint method include Lardner [19], Zhang *et al.* [29], Ayoub [43], Gejadze *et al.* [44]

Copyright © 2007 John Wiley & Sons, Ltd.

DOI: 10.1002/fld

and Gejadaz and Copeland [45]. The work of Lardner discussed the optimal control of OBC in the channel using a 2-D adjoint tidal model [19]. In the work of Zhang *et al.*, lateral tidal OBCs that force tides in the internal region are estimated by assimilating predicted coastal tidal elevations into a 2-D POM using the adjoint method [29]. Using the adjoint version of MITGCM, Ayoub carried out experiments to test whether OBC can be constrained by observations inside the domain [43]. Gejadze *et al.* and Gejadaz and Copeland studied the open boundary control problem for free-surface barotropic Navier–Stokes equations with adjoint assimilation technology [44, 45].

It is assumed that the water level at the nth time step on the open boundaries is given by

$$\zeta^n_{O_l,P_l} = a_{0,l} + [a_l \cos(\omega n \Delta t) + b_l \sin(\omega n \Delta t)]$$

where (O_l, P_l) stands for the grid points of open boundaries, ω is the frequency of M_2 constituent and a_l and b_l are the Fourier coefficients. The gradients of cost function with respect to a_l and b_l are deduced from $\partial L/\partial a_l = 0, \partial L/\partial b_l = 0$, which yields $\partial J/\partial a_l + \sum_n T^n_l \cos(\omega n \Delta t) = 0$ and $\partial J/\partial b_l + \sum_n T^n_l \sin(\omega n \Delta t) = 0$, where

$$\begin{aligned}
T^n_l &= -g\tau^n_{O_l,P_l}/a\Delta\lambda \quad \text{(for } (O_l, P_l) \text{ on the right of the area calculated)} \\
T^n_l &= g\tau^{\mathrm{j}}_{O_l-1,P_l}/a\Delta\lambda \quad \text{(for } (O_l, P_l) \text{ on the left of the area calculated)} \\
T^n_l &= -g\delta^n_{O_l,P_l}/R\Delta\phi \quad \text{(for } (O_l, P_l) \text{ under the area calculated)} \\
T^n_l &= g\delta^n_{O_l,P_l-1}/R\Delta\phi \quad \text{(for } (O_l, P_l) \text{ above the area calculated)}
\end{aligned}$$

Because the cost function decreases along the opposite direction of the gradient, we can obtain the correction of the independent BFC as

$$\begin{aligned}
K_a(a_l - a'_l) + (\partial J/\partial a_l)/\|\partial J/\partial a\|_2 = 0 \\
K_b(b_l - b'_l) + (\partial J/\partial b_l)/\|\partial J/\partial b\|_2 = 0
\end{aligned}$$

where $\|\partial J/\partial a\|_2 = (\sum_l (\partial J/\partial a_l)^2)^{1/2}$, $\|\partial J/\partial b\|_2 = (\sum_l (\partial J/\partial b_l)^2)^{1/2}$ and a'_l and b'_l are the prior values of Fourier coefficients which are given by experiences, K_a and K_b are the smoothness of OBCs in the iteration which are taken as 20.0 in this paper.

3.2.3. Optimization of vertical eddy viscosity profile. The first application of adjoint method to estimate vertical eddy viscosity profile was performed by Yu and O'Brien [14] who estimated the eddy viscosity and surface drag coefficients in a horizontally uniform ocean model and this work was extended by Richardson and Panchang [33]. On tidal models the works include Lardner and Das [20] and Lardner and Song [21] who carried out parameter estimation in a quasi-3-D tidal model. However, in their model the bottom friction is expressed in terms of depth-integrated velocities and the horizontal shear stresses and the convective terms are neglected, which are different from the model in this paper.

In the present study, the viscosity coefficients, Av, are defined at the interface between two adjacent layers. From $\partial L/\partial Av_k = 0$ we can obtain the gradient of cost function with respect to Av

Copyright © 2007 John Wiley & Sons, Ltd.

DOI: 10.1002/fld

as follows:

$$\partial J/\partial Av_k + \sum_{m,i,j}\left[\frac{\mu^m_{i+1/2,j,k}(u^m_{i+1/2,j,k}-u^m_{i+1/2,j,k+1})}{\Delta z_{i+1/2,j,k}\Delta z_{i+1/2,j,k+1/2}} - \frac{\mu^m_{i+1/2,j,k+1}(u^m_{i+1/2,j,k}-u^m_{i+1/2,j,k+1})}{\Delta z_{i+1/2,j,k+1}\Delta z_{i+1/2,j,k+1/2}}\right]$$

$$+\sum_{m,i,j}\left[\frac{\gamma^m_{i,j+1/2,k}(v^m_{i,j+1/2,k}-v^m_{i,j+1/2,k+1})}{\Delta z_{i,j+1/2,k}\Delta z_{i,j+1/2,k+1/2}} - \frac{\gamma^m_{i,j+1/2,k+1}(v^m_{i,j+1/2,k}-v^m_{i,j+1/2,k+1})}{\Delta z_{i,j+1/2,k+1}\Delta z_{i,j+1/2,k+1/2}}\right]=0$$

The correction of Av can then be obtained as

$$K_v(Av_k-\hat{A}v_k)+(\partial J/\partial Av_k)/\|\partial J/\partial Av\|_2=0$$

i.e.

$$Av_k=\hat{A}v_k-\frac{1}{K_v}(\partial J/\partial Av_k)/\|\partial J/\partial Av\|_2=0$$

where

$$\|\partial J/\partial Av\|_2=\left(\sum_k(\partial J/\partial Av_k)^2\right)^{1/2}$$

where Av_k, $\hat{A}v_k$ are prior and optimized values of eddy viscosity coefficients, respectively, K_v is the coefficient that represents the smoothness of eddy viscosity profile in the iteration process and K_v is taken as 10^4 in the model which is obtained through a trial-and-error procedure.

4. NUMERICAL EXPERIMENTS AND RESULTS ANALYSIS

4.1. Computing area and data

The computing area in the present study is BNYS, a semi-closed sea between China and the Korean Peninsula (Figure 3). The space resolution in this model is $1/6^\circ \times 1/6^\circ$. The angular frequency of M_2 tide is $1.405189025\times10^{-4}\,\mathrm{s}^{-1}$ and the time step of external mode is 372.618 s (1/120 of the period of M_2 tide) and the time step of internal mode is 1490.472 s, four times that of external mode. T/P altimeter data, tidal gauge data and ship-measured current data are assimilated into the adjoint tidal model. The tidal gauge data and the T/P process are described by Lu and Zhang [31]. The bathymetry map of BNYS, the position of T/P satellite tracks, tidal stations, current observations and open boundaries are all shown in Figure 3. The tide gauge data of this paper are taken from coastal and island tide stations; hence, in Figure 3 one can find some stations locate significant distances from the coast. Besides, in the present study we use 10 years of T/P altimeter data from the beginning of the T/P mission in September 1992 to the completion in September 2002. The harmonic constants of M_2 tidal flow are obtained form ship-measured current data (8 days long, hourly data). The tide gauge data are generally based on at least one-year observation and thus are sufficiently accurate. It should be noted that the experiments in this paper are identical twin ones; hence, only the position of observations is used and the values are obtained by running the original dynamic forward model.

Copyright © 2007 John Wiley & Sons, Ltd.

DOI: 10.1002/fld

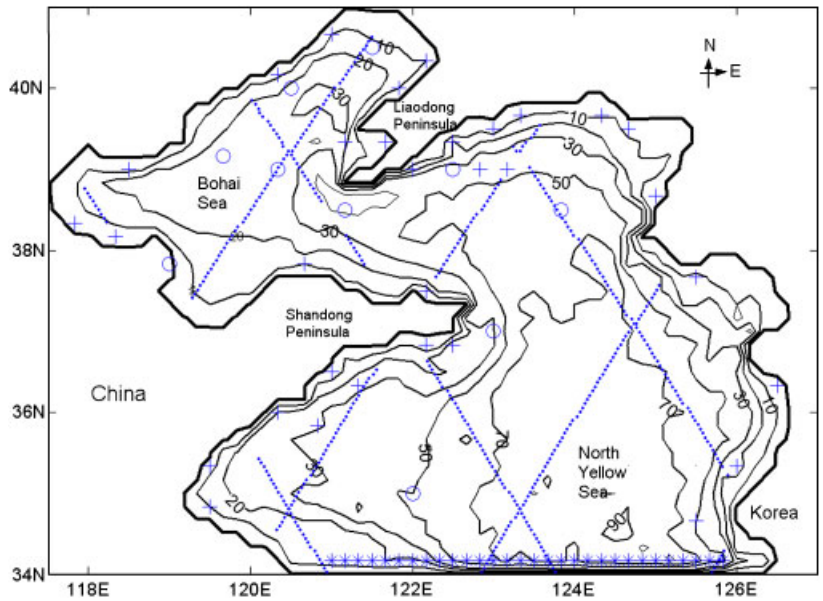

Figure 3. The bathymetric map of BNYS and the position of T/P satellite tracks, tidal stations, current observations and open boundaries. The dots are the grid points under T/P satellite tracks. The open circles indicate the current observations. The symbol '+' denotes the coastal and island tidal stations and '$*$' stands for the open boundaries.

4.2. Numerical experiments

In this section, the identical twin experiments will be carried out to test the inversion ability and effectiveness of the adjoint model. Lardner and Das [20] and Lardner and Song [21] also designed twin experiments for their quasi-3-D adjoint tidal model; however, in their work the computing area and ocean topography are both idealized. As we know, the topography in the ocean model is the most fundamental factor. Therefore, in the twin experiments of this paper, the real topography of BNYS is installed.

The twin experiments are designed as follows. First, a certain distribution of a kind of parameters is prescribed. Then the forward tidal model is run using the prescribed distributions and the simulation results at the position of observed data shown in Figure 3 are taken as the 'observations' of twin experiments, i.e. only the position of the observed data is used and the values are obtained by running the original dynamic forward model. Having obtained the 'observations', an initial value is assigned to the parameter to be inverted and the forward simulation is performed. The difference in water elevation and current velocity between simulated values and 'observations' serves as the external force of the adjoint model. The optimized parameters can be obtained through the backward integration of the adjoint equations. The inverse integral time of the adjoint equations is equal to a period of M_2 tide. With the above procedure repeated, the parameters will be optimized continuously and the difference between simulated values and 'observations' will be diminished. Meanwhile, the difference between the prescribed and the inverted parameters will also be decreased. Following sections will describe the inversion of OBC, BFC and vertical eddy viscosity profile, respectively.

Copyright © 2007 John Wiley & Sons, Ltd.

DOI: 10.1002/fld

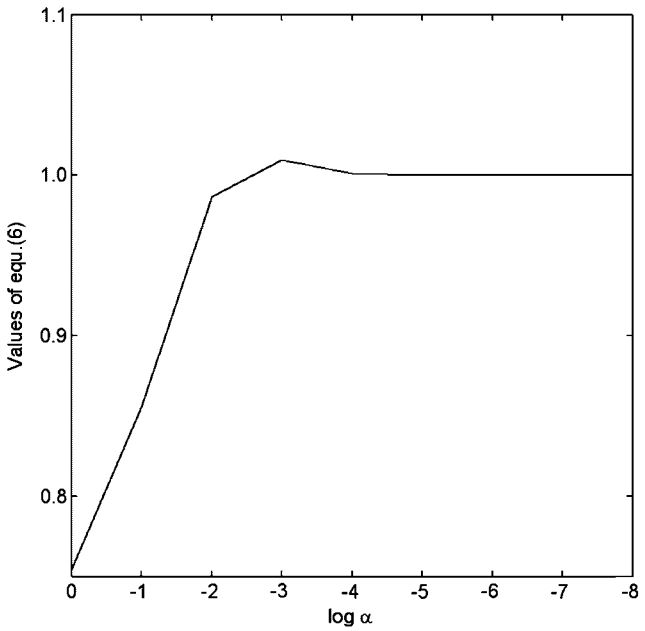

Figure 4. Values of the function $\Phi(\alpha)$ *versus* α.

It is important to obtain the right gradient of the cost function with respect to the model parameters. Let

$$J(P+\alpha U)=J(P)+\alpha U\nabla_P J(P)+\text{h.o.t.} \tag{11}$$

be a Taylor expansion of the cost function (10) in Section 3.1, where P is a parameter, α is a small scalar and U is an arbitrary vector of unit length. Rewriting (11) we can define a function of α given by

$$\Phi(\alpha)=\frac{J(P+\alpha U)-J(P)}{\alpha U\nabla_P J(P)} \tag{12}$$

As mentioned in the work of Smedstad and O'Brien [13], Das and Lardner [17], Lardner and Das [20] and Lardner and Song [21], if α is chosen close to the machine zero one cannot expect to be able to verify that the correct gradient has been found. For values of α which are not too close to the machine zero, one should expect to obtain a value for $\Phi(\alpha)$ which is close to 1. In Figure 4, we plot the values of $\Phi(\alpha)$ when the BFCs are taken as the example. It can be seen that for α between 10^{-3} and 10^{-8}, $\Phi(\alpha)$ is close to 1, which means that the correct gradient is therefore found.

4.2.1. Inversion of open boundary conditions. In this section, the Fourier coefficients of OBC at 30 grid points shown in Figure 3 are inverted. The 'true values' of Fourier coefficients are taken from Lu and Zhang [31] in which the M_2 tide in BYECS is simulated using a 2-D adjoint tidal model. Three groups of experiments are carried out. Group 1 discusses the influence of initial guesses on inversion results and the initial guesses for cases 1–5 in this group are 0, 0.1, -0.1, 0.2 and -0.2, respectively. Group 2 tests the effect of noisy data. To do this, we have replaced

Copyright © 2007 John Wiley & Sons, Ltd.

DOI: 10.1002/fld

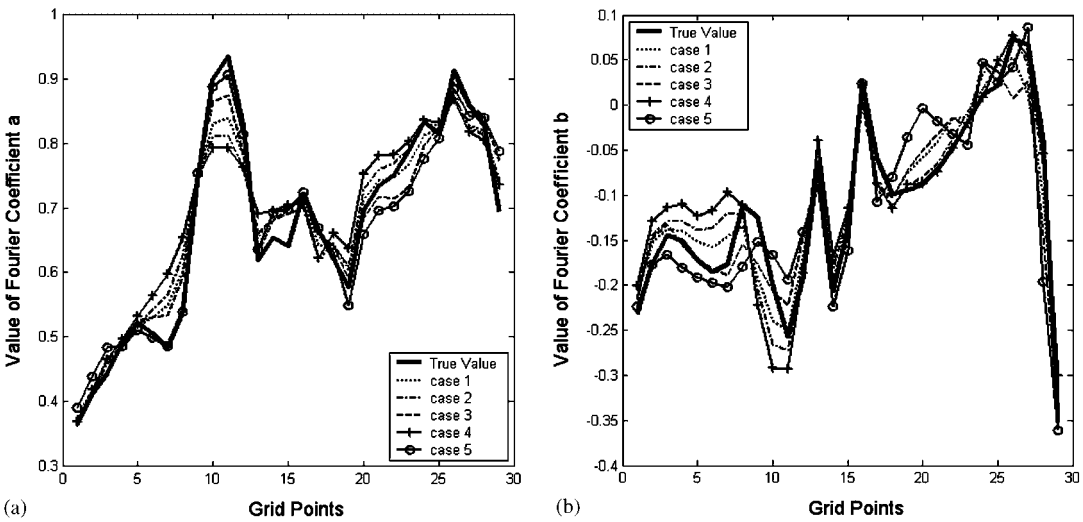

Figure 5. Inverted OBC for different initial guesses.

each 'observations' $\hat{\zeta}^n_{i,j}$, $\hat{u}^m_{i,j,k}$ and $\hat{v}^m_{i,j,k}$ by $(1+pr^n_{i,j})\hat{\zeta}^n_{i,j}$, $(1+pr'^m_{i,j,k})\hat{u}^m_{i,j,k}$ and $(1+pr'^n_{i,j,k})\hat{v}^m_{i,j,k}$, respectively, where $r^n_{i,j}$ and $r'^m_{i,j,k}$ are uniform random numbers lying in $(-1, 1)$ and p is a factor determining the maximum percentage error. The maximum percentage errors for cases 6–11 in this group are 3, 6, 10, 13, 16 and 20%, respectively. The relation between the number of 'observation' and the inversion result is researched by cases 1, 12 and 14 in Group 3. For case 1, the T/P 'observations', the tidal gauge 'observations' and the current 'observations' are all assimilated, and for case 12 the current 'observations' are not employed. For case 13 only the T/P 'observations' are used, and for case 14 only the 'observations' of tidal stations are assimilated. The inversion results of Groups 1–3 are plotted in Figures 5–7, respectively. The average differences between 'true values' and inversion results before and after assimilation are shown in Table I. Figure 8 gives the values of cost function J and J/J_0 *versus* iteration steps in these cases, where J_0 is the value of cost function at the first iteration step. The correlation coefficients between 'true values' and inversion results are also given in Table I.

From Figures 5–7, one can find that the prescribed OBCs have been successfully inverted in all cases. This conclusion can also be shown by Table I in which the correlation coefficients are all larger than 0.85 and the average differences between 'true values' and inversion results are decreased significantly after assimilation. In Group 1, the influence of initial guess is studied and the correlation coefficients all are larger than 0.93, which indicates that the prescribed OBC distributions have been inverted successfully. The model in this paper is nonlinear and the cost function for a nonlinear model is not guaranteed to possess a single minimum. We should find the global minimum but not a local one. We use very different initial guesses and all the solutions can converge to the correct one (Figure 5). Meanwhile, Figure 8 shows that by using different initial guesses the cost function can reach almost the same minimum. However, the new estimates of the parameters will not deviate far from the values taken by the parameters at the previous iteration. Therefore, in this sense the parameters' initial guess should be as reasonable as possible so that the optimization process can perform efficiently (see, Reference [14]). The effect of observation

Copyright © 2007 John Wiley & Sons, Ltd.

DOI: 10.1002/fld

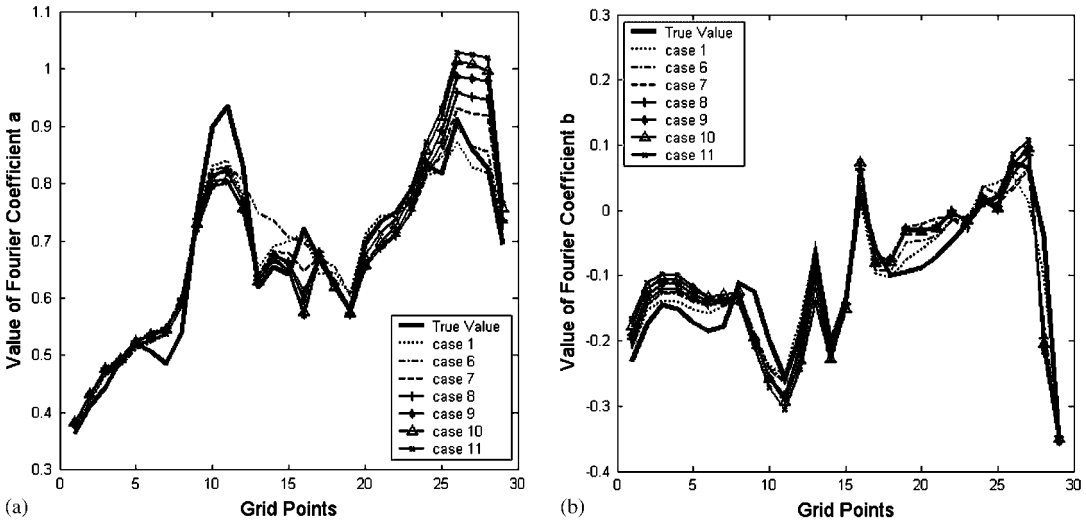

Figure 6. Inverted OBC for different random errors.

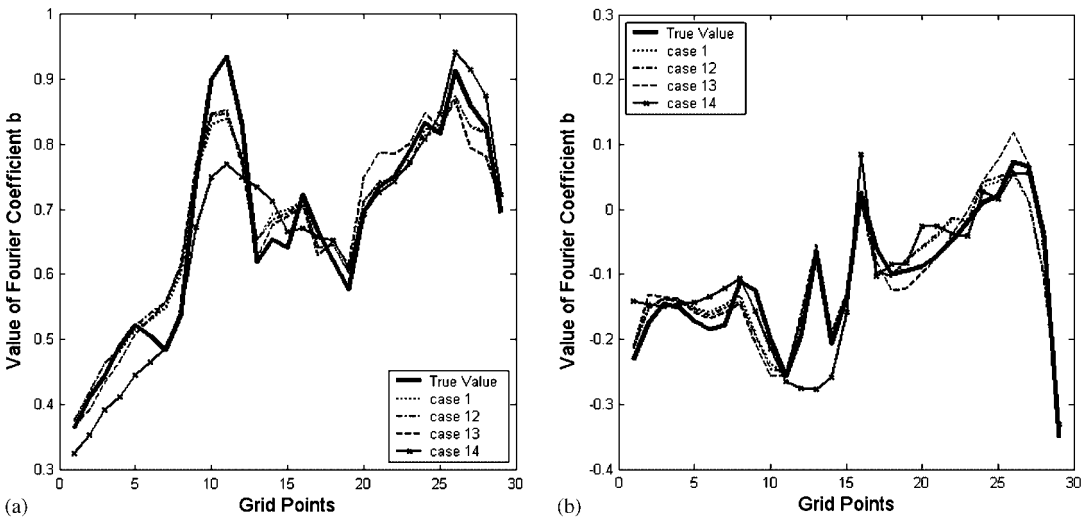

Figure 7. Inverted OBC for different number of 'observations'.

error is discussed in Group 2. The minimum value of correlation coefficients of this group is 0.88 for case 11 in which the maximum percentage error is 20%. We can conclude that, when the observation error is taken into account, the model can converge the solutions to the correct one. In some works researchers proposed to insert an additional criterion into the cost function named the penalty term, which can penalize large fluctuations in the estimated parameters to ensure that parameters vary smoothly. Lardner and Das [20] pointed out that this term was useful especially

Copyright © 2007 John Wiley & Sons, Ltd.

DOI: 10.1002/fld

Table I. The average difference between 'true values' and inversion results of Fourier coefficients before and after assimilation.

	Case information			Average difference		
Exp.	Initial guess	Random error (%)	Data number	Before assimilation	After assimilation	Correlation coefficient
Case 1	0.0	0	Full	0.400	0.027	0.97
Case 2	0.1	0	Full	0.393	0.029	0.96
Case 3	−0.1	0	Full	0.428	0.026	0.98
Case 4	0.2	0	Full	0.393	0.037	0.93
Case 5	−0.2	0	Full	0.491	0.029	0.94
Case 6	0.0	3	Full	0.400	0.032	0.94
Case 7	0.0	6	Full	0.400	0.036	0.93
Case 8	0.0	10	Full	0.400	0.040	0.91
Case 9	0.0	13	Full	0.400	0.043	0.90
Case 10	0.0	16	Full	0.400	0.047	0.89
Case 11	0.0	20	Full	0.400	0.051	0.88
Case 12	0.0	0	No cur. obs.	0.400	0.027	0.97
Case 13	0.0	0	No TS. and cur. obs.	0.400	0.029	0.96
Case 14	0.0	0	No T/P and cur. obs.	0.400	0.051	0.85

when the data contain observation error. However, the results of Group 2 indicate that the method described in Section 3.2 can also conquer this difficulty. Meanwhile, the larger the maximum percentage error becomes, the bigger the difference will be, which can be expected. The number of 'observations' is changed in Group 3 and the result shows that the OBC can be inverted only with the tidal gauge 'observations'. It indicates that the data in this paper, especially the large amount of T/P data, are able to constrain the OBC inversion problem. However, as shown by Figure 7, the result of case 14 has been much worse than those using more 'observations', which can also be indicated by the smallest correlation coefficient 0.85 in Table I. Figure 8 shows that the values of J and J/J_0 have been greatly decreased, which demonstrates the strong inverse ability of this model.

4.2.2. Inversion of bottom friction coefficients. In this section, the BFC distributions are prescribed and then are inverted by the model. As described in Section 3.2.1, the BFCs are supposed to be spatially varying. In fact, as shown by the work of Zhang *et al.*, if the BFC distributions are complicated in space, the spatially varying BFC is the only way that can successfully invert the given distributions (see, Reference [46]). Two types of BFC distributions including the revolution conical surface distribution (ruled surface) and the revolution parabolic surface distribution (quadric surface) are prescribed. Considering the convex direction, there are four prescribed distributions totally, which are shown in Figure 9. According to the previous works on the BFC in BNYS, all the prescribed BFCs are between 0.001 and 0.003. Four groups of experiments are carried out. Cases 1–4 in Group 1 invert the four prescribed distributions, respectively, and the first distribution of Figure 9 is taken as the example to be inverted in the other three groups. In Group 2, cases 1 and 5–7 discuss the impact of initial guesses on inversion results and the initial guesses for these cases are 0.002, 0.001, 0.0015 and 0.0025, respectively. Group 3 tests the effect of data noise and the maximum percentage errors for cases 8–10 in this group are 4, 8 and 10%, respectively. The relation between the number of 'observations' and the inversion results is researched by cases 1

Copyright © 2007 John Wiley & Sons, Ltd.

DOI: 10.1002/fld

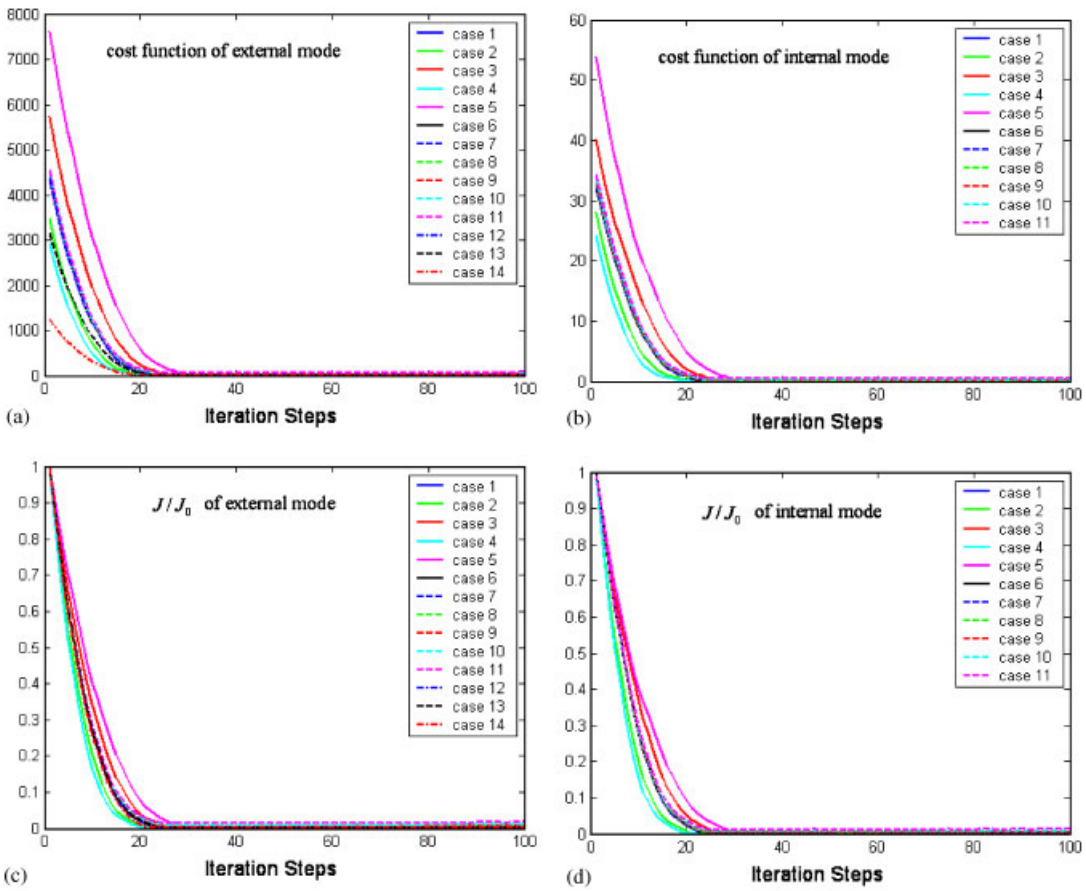

Figure 8. The values of J and J/J_0 *versus* the iteration steps.

and 11–13 in Group 4. For case 1 all the 'observations' are used, and for case 11 the current 'observations' are not employed. For case 12 only the T/P 'observations' are assimilated, and for case 13 only the 'observations' of tidal stations are installed. The inversion results of Groups 1–4 are plotted in Figures 10–13, respectively. The average differences between 'true values' and inversion results before and after assimilation are shown in Table II and so are the correlation coefficients. Figures 14–17 give the contour maps of differences for Groups 1–4 between prescribed and inverted distributions, respectively.

In this section, the prescribed BFC distributions are inverted and the inversion results indicate that the adjoint model has a strong ability to invert the BFC by optimizing the spatially varying BFC. The complicate BFC distributions are inverted successfully in all cases. All the correlation coefficients are larger than 0.93 except case 10. Obviously the inversion would not succeed if the BFCs were supposed to be a constant over the whole domain or different constants in different subdomains. In Group 1 the four different distributions are inverted by cases 1–4, respectively, and we can get the following details based on the inversion results. For surfaces of different types,

Copyright © 2007 John Wiley & Sons, Ltd.

DOI: 10.1002/fld

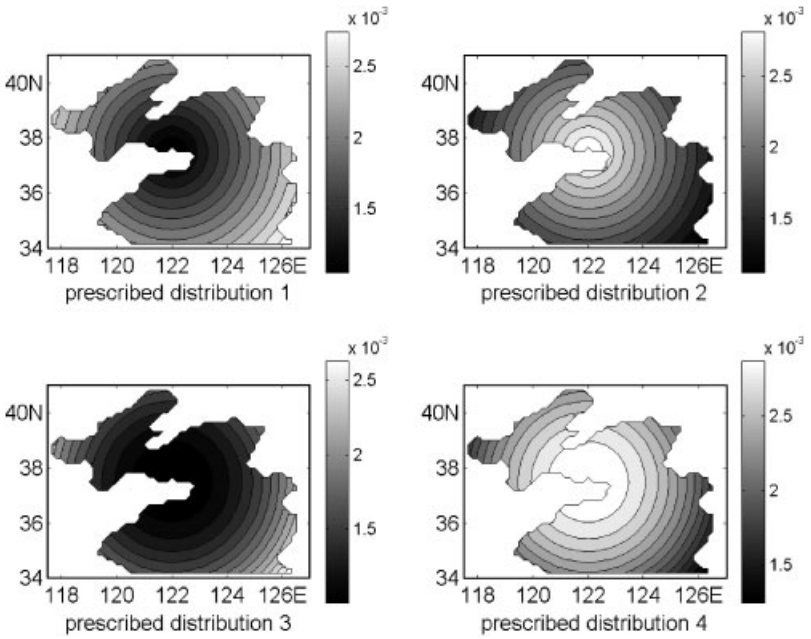

Figure 9. The four prescribed BFC distributions.

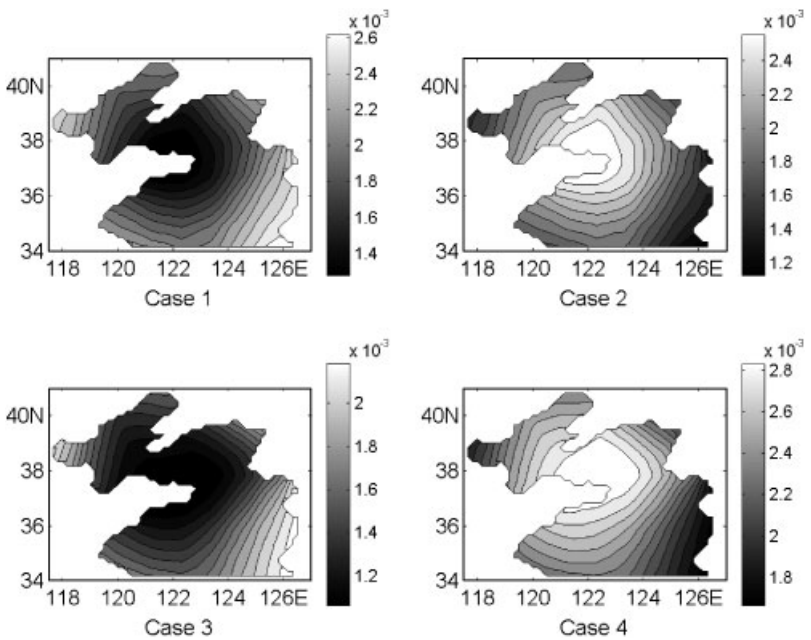

Figure 10. Inverted BFC for different distributions.

Copyright © 2007 John Wiley & Sons, Ltd.

DOI: 10.1002/fld

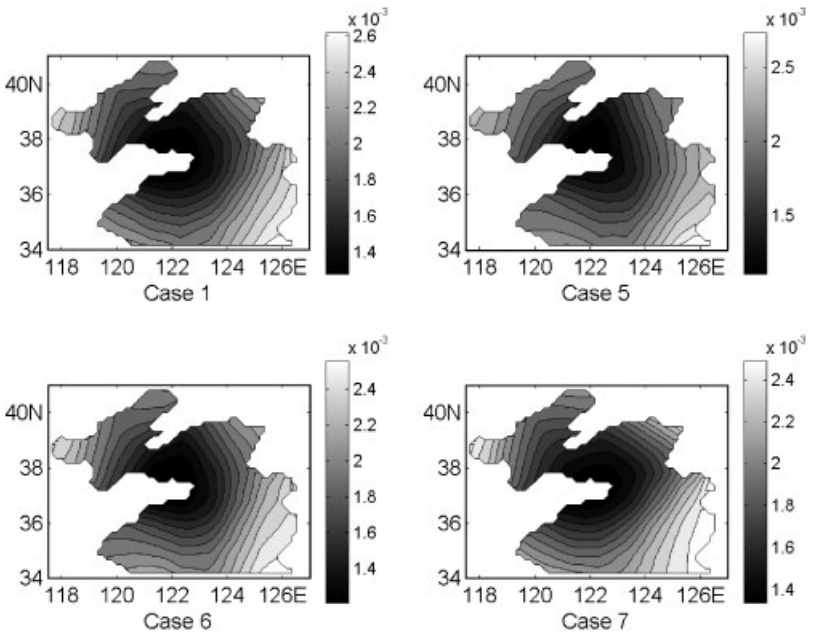

Figure 11. Inverted BFC for different initial guesses.

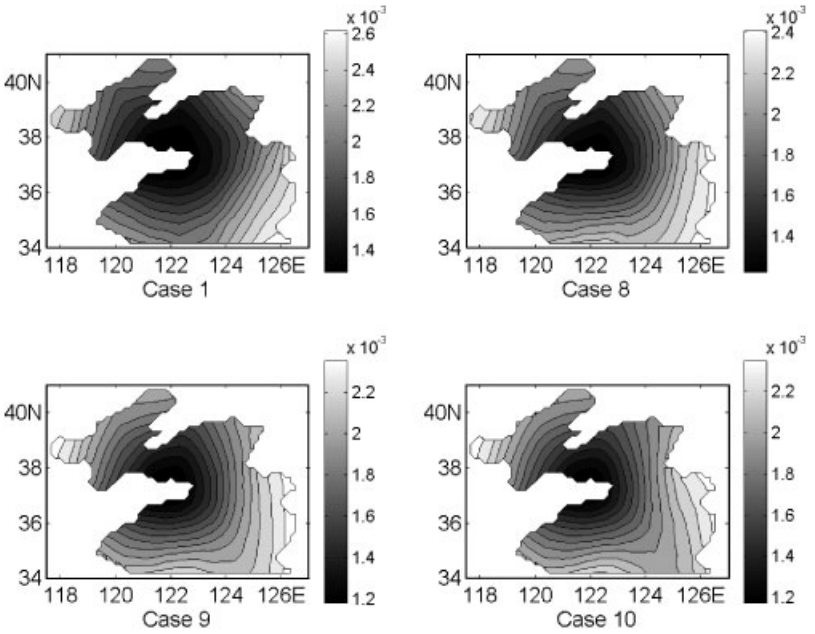

Figure 12. Inverted BFC for different random errors.

Copyright © 2007 John Wiley & Sons, Ltd.

DOI: 10.1002/fld

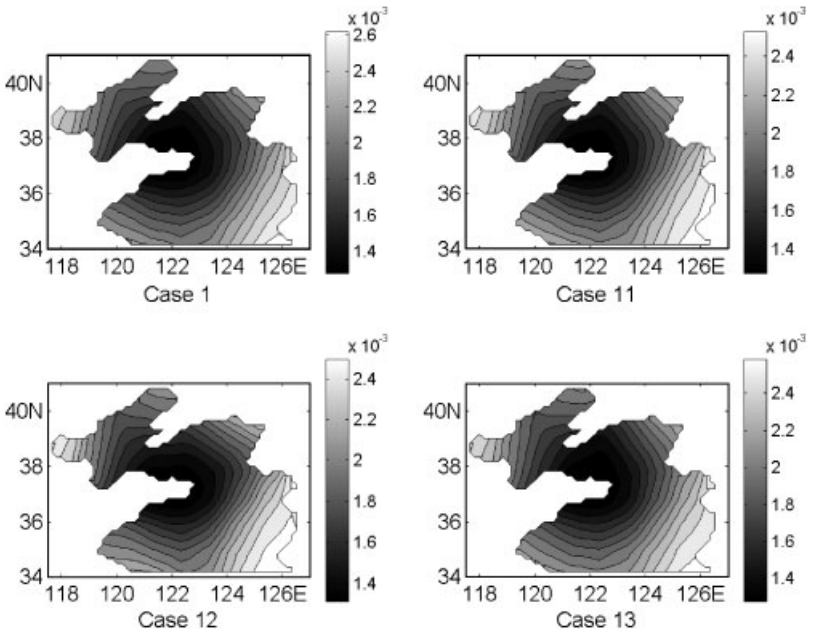

Figure 13. Inverted BFC for different number of 'observations'.

Table II. The average difference between 'true values' and inversion results of BFC before and after assimilation.

	Case information			Average difference		
Exp.	Initial guess	Random error (%)	Data number	Before assimilation	After assimilation	Correlation coefficients
Case 1	0.002	0	Full	2.90E−04	3.74E−05	0.99
Case 2	0.002	0	Full	2.90E−04	4.14E−05	0.98
Case 3	0.002	0	Full	5.60E−04	9.57E−05	0.93
Case 4	0.002	0	Full	5.60E−04	9.91E−05	0.92
Case 5	0.001	0	Full	9.07E−04	5.79E−05	0.98
Case 6	0.0015	0	Full	4.51E−04	4.66E−05	0.98
Case 7	0.0025	0	Full	6.03E−04	8.43E−05	0.95
Case 8	0.002	4	Full	2.90E−04	5.82E−05	0.97
Case 9	0.002	8	Full	2.90E−04	7.43E−05	0.93
Case 10	0.002	10	Full	2.90E−04	9.12E−04	0.81
Case 11	0.002	0	No cur. obs.	2.90E−04	4.33E−05	0.98
Case 12	0.002	0	No TS. and cur. obs.	2.90E−04	4.36E−05	0.98
Case 13	0.002	0	No T/P and cur. obs.	2.90E−04	6.32E−05	0.97

the inversion results of revolution conical surfaces are better than those of revolution parabolic surfaces. We think the reason is that the revolution parabolic surfaces are more complicated than the conical ones. For surfaces of the same type, the inversion results of the upward convex surfaces are better than those of the downward ones. Perhaps, it is because the upward convex surface

Copyright © 2007 John Wiley & Sons, Ltd.

DOI: 10.1002/fld

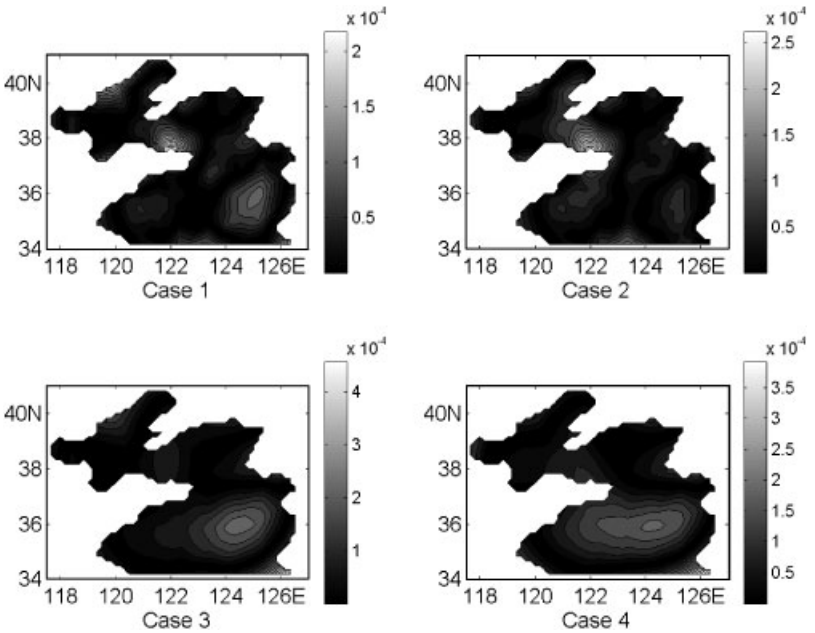

Figure 14. The differences between prescribed BFC and inversion results for Group 1.

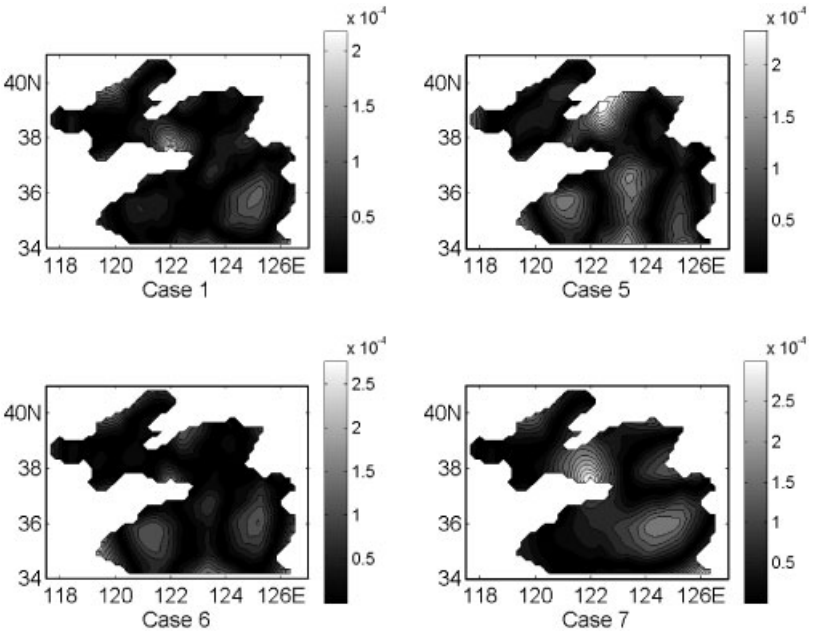

Figure 15. Same as Figure 14, but for Group 2.

Copyright © 2007 John Wiley & Sons, Ltd.

DOI: 10.1002/fld

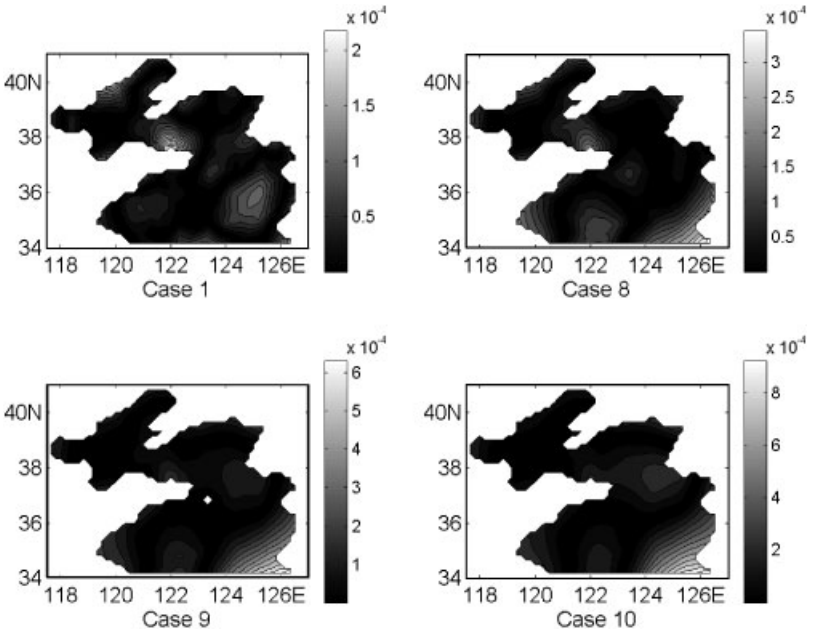

Figure 16. Same as Figure 14, but for Group 3.

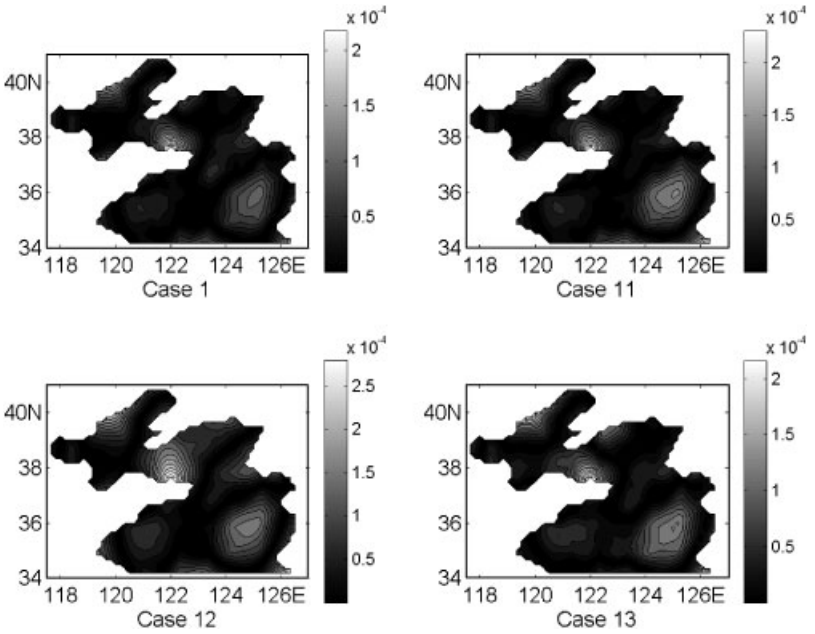

Figure 17. Same as Figure 14, but for Group 4.

Copyright © 2007 John Wiley & Sons, Ltd.

DOI: 10.1002/fld

distributions are more reasonable to adapt to the real ocean topography. The same phenomenon has been pointed out in the work of Lu and Zhang [31]. The conclusions deduced from Groups 2 and 4 are similar to those of Section 4.2.1. In Group 2 we change the initial guesses and all the solutions have converged to the correct one (Figure 11), which can be proved by the correlation coefficients that are larger than 0.95 for case 7. In Group 4, when the number of data is reduced, the BFC can still be inverted successfully, even when only the tidal gauge data are used. In this paper, the independent BFCs are selected uniformly over each $1^\circ \times 1^\circ$ area and the number of independent BFCs is a result of a trial-and-error procedure. Therefore, based on the results of Group 4, we can state that the amount of data is plenty enough to constrain the BFC inversion problem. However, if random errors are introduced into the 'observations', the inversion results of BFC are not as good as those of OBC. In Section 4.2.1, when the maximum percentage error is 20%, the inversion results are still satisfactory and the correlation coefficient is 0.85. In this section, the correlation coefficient is 0.81 for case 10 when the maximum percentage error is 10%. It indicates that the inversion of BFC might be unbelievable if the error gets larger than 10%. Thus, we can conclude that the inversion of BFC is more sensitive to data noise than that of OBC.

4.2.3. Inversion of vertical eddy viscosity profile. In this section, four groups of experiments are carried out to invert the prescribed vertical eddy viscosity profiles. The number of vertical levels inside the water column is taken as 8. In Group 1, four kinds of distributions are prescribed and they are inverted by cases 1–4, respectively. In Group 2, cases 5–11 discuss the impact of noisy data on inversion results and the maximum percentage errors for these cases are 0, 3, 5, 8, 10, 13 and 15%, respectively. Group 3 tests the effect of initial guesses and the initial guesses for case 1, case 5 and case 12 in this group are 0.002, 0.0055 and 0.0038, respectively. The relation between the number of 'observations' and the inversion results is studied by cases 2, 13 and 14 in Group 4. For case 2 all the 'observations' are assimilated. For case 13 only the 'observations' of tidal stations and one current 'observation' are employed, and the number of current 'observation' is three for case 14. The inversion results of Groups 1–4 are plotted in Figures 18–21, respectively. The average differences between 'true values' and inversion results before and after assimilation are shown in Table III, where the correlation coefficients are also exhibited.

The inversion of vertical eddy viscosity coefficients has obtained satisfactory results. From Table III one can find that after assimilation the average differences have been decreased greatly and the correlation coefficients between inversion results and prescribed distributions all are larger than 0.87. In Group 1 the four different prescribed distributions are inverted. The results of cases 1 and 2 are better than those of cases 3 and 4. The most probable reason is that the first and the second distributions are simpler than the other two. The effect of data noise is tested in Group 2 and from Figure 19 we can find that when the maximum percentage error is less than 10%, only a tiny difference lies among the inversion results of cases 5–9. However, when the maximum percentage error is increased from 10 to 13% of case 10, the average differences between inversion results and 'true values' sharply increased from 1.55E−04 to 2.96E−04, while the correlation coefficient decreased from 0.98 to 0.90. But we think the results of cases 10 and 11 are still reasonable. Group 3 discusses the influence of initial guesses on inversion and the correlation coefficients for cases 1, 5 and 12 are 0.98, 0.99 and 0.98, respectively. In addition, the large correlation coefficients demonstrate that the data used are plenty to constrain the eddy viscosity coefficient inversion problem in this section. The results of Group 4 can be expected. In cases 13 and 14, the T/P 'observations' are excluded and the number of current 'observations' are 1 and 3, respectively. The inversion result of case 14 is satisfactory and the correlation coefficient equals that of case

Copyright © 2007 John Wiley & Sons, Ltd.

DOI: 10.1002/fld

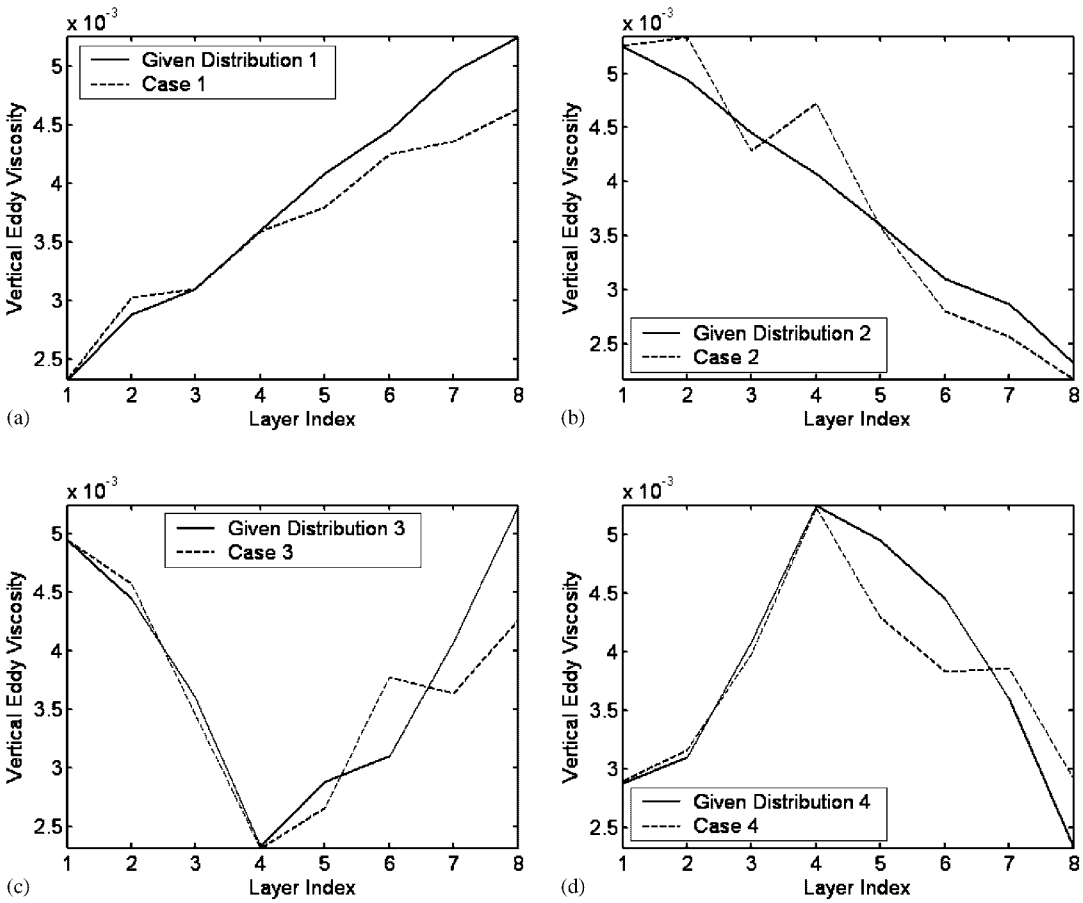

Figure 18. Inverted vertical eddy viscosity coefficient for different distributions.

2 in which all the 'observations' are used. However, Figure 21 indicates that when the number of current 'observations' is decreased to 1, the inversion result of case 13 has been distorted and the correlation coefficient is sharply decreased from 0.98 to 0.87. We calculate the average difference of each layer in all cases and the values from the surface layer to the bottom layer are 3.23E−5, 1.39E−4, 5.06E−5, 1.08E−4, 2.45E−4, 2.81E−4, 1.99E−4 and 2.23E−4, respectively. Obviously, the inversion results of the upper four layers are better than those of the other four layers. However, in the work of Richardson and Panchang, they put forward a problem that if the wind forcing was absent and the model was driven by tidal forcing alone, they could not obtain good estimates of eddy viscosity except at lower levels of the water column [33]. The reason for this is probably that the models used in two works are different. The model for their work is a coastal circulation model. The better inversion for the upper layers in this paper, we guess, may be due to the using of large amount of surface elevation data. If the sea surface elevation can be simulated accurately, it will benefit the whole adjoint system.

Copyright © 2007 John Wiley & Sons, Ltd.

DOI: 10.1002/fld

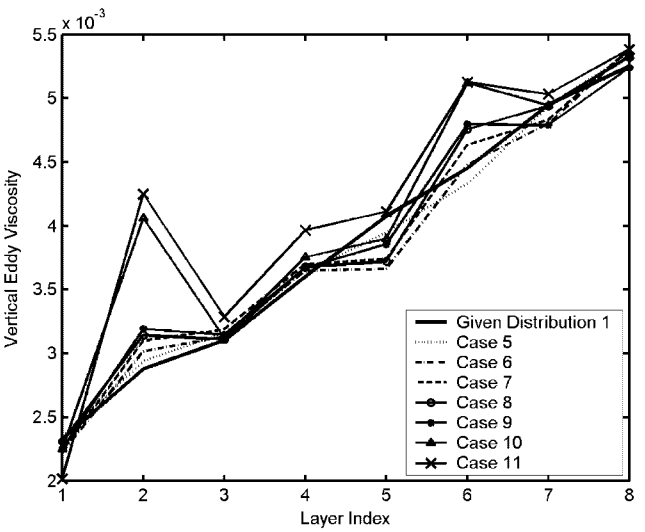

Figure 19. Inverted vertical eddy viscosity coefficient for different random errors.

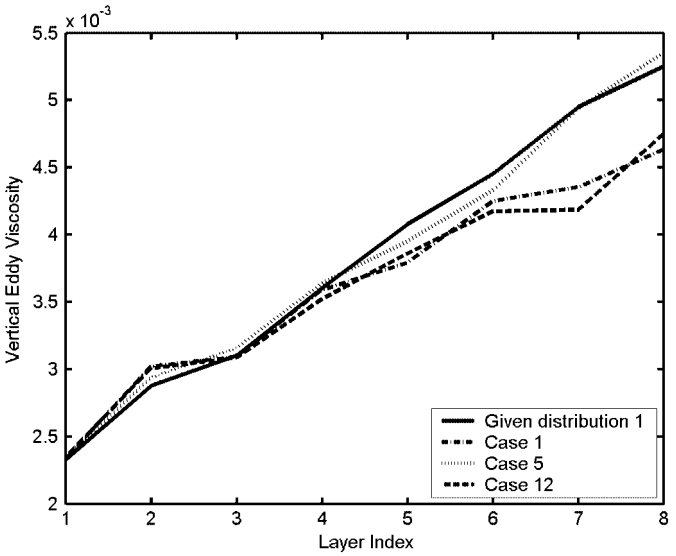

Figure 20. Inverted vertical eddy viscosity coefficient for different initial guesses.

4.3. Discussion on the numerical experiments

In Section 3.2.1, the coefficient K_c represents the smoothness in the iterative process. In our model the gradient $\partial L/\partial b_{ii,jj}$ is normalized first by $\|\partial J/\partial b\|_2$, which means that mainly the direction of the gradient is used when the optimization is performed. A small positive value is assigned to $1/K_c$ in order to ensure that cost function can decrease continuously without large fluctuations

Copyright © 2007 John Wiley & Sons, Ltd.

DOI: 10.1002/fld

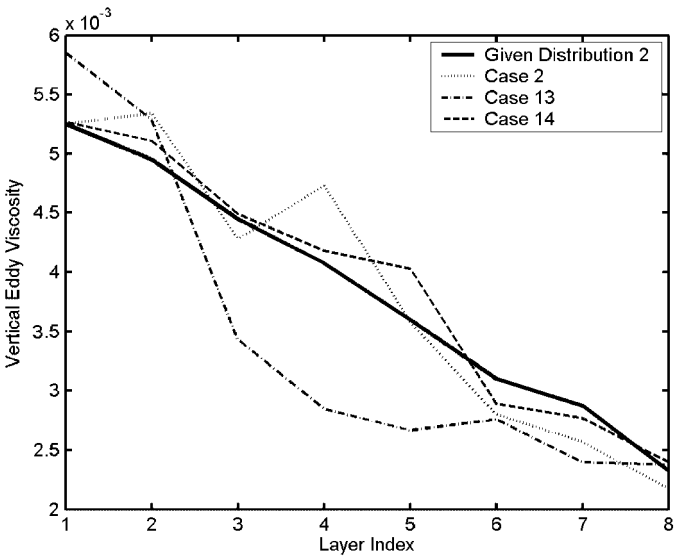

Figure 21. Inverted vertical eddy viscosity coefficient for different number of 'observations'.

Table III. The average difference between 'true values' and inversion results of vertical eddy viscosity coefficients before and after assimilation.

	Case information			Average Difference		
Exp.	Initial guess	Random error (%)	Data number	Before assimilation	After assimilation	Correlation coefficient
Case 1	0.002	0	Full	1.83E−03	2.33E−04	0.98
Case 2	0.002	0	Full	1.83E−03	2.49E−04	0.98
Case 3	0.002	0	Full	1.83E−03	3.26E−04	0.89
Case 4	0.002	0	Full	1.83E−03	2.90E−04	0.93
Case 5	0.0055	0	Full	1.67E−03	6.69E−05	0.99
Case 6	0.0055	3	Full	1.67E−03	1.30E−04	0.98
Case 7	0.0055	5	Full	1.67E−03	1.59E−04	0.98
Case 8	0.0055	8	Full	1.67E−03	1.39E−04	0.98
Case 9	0.0055	10	Full	1.67E−03	1.55E−04	0.98
Case 10	0.0055	13	Full	1.67E−03	2.96E−04	0.90
Case 11	0.0055	15	Full	1.67E−03	3.95E−04	0.88
Case 12	0.0038	0	Full	8.53E−04	2.50E−04	0.98
Case 13	0.002	0	No T/P, 1 cur. obs.	1.83E−03	6.24E−04	0.87
Case 14	0.002	0	No T/P, 3 cur. obs.	1.83E−03	1.43E−04	0.98

(see, Reference [31]). In Section 4.2.2 where the prescribed BFC distributions are inverted, $1/K_c$ is taken as 10^{-4}, i.e. $K_c = 10^4$ which is obtained through a trial-and-error procedure. K_a, K_b in Section 3.2.2 and K_v in Section 3.2.3 are taken as $20.0, 20.0$ and 10^4, respectively, which all are obtained through a trial-and-error procedure. In our model, we monitor the convergence by examining the cost function and terminate the iteration when the change of cost function

Copyright © 2007 John Wiley & Sons, Ltd.

DOI: 10.1002/fld

becomes very small. Obviously, the number of iteration steps that is needed to invert the prescribed distributions successfully is closely related to smoothness coefficients and the initial values of given parameters. In the experiments of Section 4.2, in order to compare the inversion results all the iteration processes are terminated at the 100th step because the values of cost function will decrease very slowly at this step (the difference between the values of J/J_0 of two adjoint steps has been less than 10^{-4}); therefore, it is worthless to continue the optimization. In Section 4.2.1, Figure 8 gives the values of cost function J and J/J_0 *versus* the iteration steps. One can find that around the 100th step the values of cost function are almost unchanged and nearly all the cost functions have reached the same minimum value. What should be noted is that there are no large fluctuations in the decreasing of cost function.

With identical twin experiments, the data are perfect in the sense that they are obtained from the model and thus are consistent with the model physics. However, one can find that even when we add zero noise to the observations, the model cannot produce the exact parameter estimates. In the twin experiments, we mainly discuss the inversion of three kinds of parameters in the tidal model. When one kind of parameter is inverted, we try to reduce the influence of the other factors. However, it is difficult for us to do it completely. Take the inversion of BFC for example. In the cases of Section 4.2.2, the real topography of BNYS and the 'real' OBC have been installed. Although the OBC and the topography are fixed all the time, the inversion can also be influenced by them. As we know, the BFC should dissipate the energy propagating from the open boundary to maintain the tidal system. However, the initial values of BFC are just given by experience and the prescribed BFC distributions are just the analytical function of the horizontal spatial coordinates. Therefore, the initial BFC and the inverted BFC cannot suit the 'real' M_2 tide in the process of inversion exactly and the inversion must have been distorted. That is to say, the BFC is the major but not the unique determining factor in the inversion of Section 4.2.2. Thus from Figures 10–13, one can find that the inversion results are not exactly equal to the prescribed BFC and there is a large amount of small-scale variability that is not present in Figure 9. We have done a case where the uniform boundary forcing is applied and the two Fourier coefficients are taken as the parameters and estimated, and the results demonstrate that the two parameters can be inverted exactly. In this case the prescribed values of both Fourier coefficients are 0.2, the maximum percentage error is 20%, the initial value is 0.4 and the data used are just the tidal gauge data. The model has produced the exact parameter estimation. As the boundary forcing becomes more spatially variable (thus requiring more parameters), the inversion would become less exact, which can be expected. In the work of Smedstad and O'Brien where the spatially distributed phase speed in an equatorial Pacific Ocean model was estimated, they could not produce the exact values either, even when perfect observations were available at every gridpoint of the model (see, Reference [13]). We think it is normal if one seeks parameters distributed in space and time domain.

Tihonov proved that if the forward model is linear in the parameters, the solution to the inverse problem exists, is unique, and depends continuously on the measurements [47, 48]. The numerical results of underground water inverse problem also demonstrate that when perfect observation is assimilated, the cost function for the linear problem is convex and thus the solution is unique. However, if the observation error is taken into account, the cost function of the inverse problem might be nonconvex and the solution might be nonunique, even when the forward model is linear. Besides, the parameter estimation problem might be beset by nonuniqueness problem if the parameters are supposed to be temporal or spatial [32]. In this paper, from the results of numerical experiments where the effect of initial guesses are discussed, one can find that the solutions using very different initial guesses have all converged to the correct one (Figures 5, 11 and 20). Therefore

Copyright © 2007 John Wiley & Sons, Ltd.

DOI: 10.1002/fld

we can state that if the observed data are perfect, the solutions to the inverse problems in this paper are unique. However, if the observed data are contaminated by the noise, the solutions could not converge to the correct one, especially when the maximum percentage error is too large (Figures 6, 12 and 19).

5. CONCLUSIONS

In this paper we construct a 3-D adjoint tidal model and the parameters of the model are estimated using the adjoint assimilation method. Among all the data assimilation methods, 4DVAR data assimilation is one of the most effective and powerful approaches. It is an advanced data assimilation method that involves the adjoint method and has the advantage of directly assimilating various observations distributed in time and space into numerical models while maintaining dynamical and physical consistency with the model. The mode splitting technique is employed in both the forward model and the adjoint model. In the external mode the ADI method is used to discretize the 2-D depth-averaged equations and a semi-implicit scheme is employed for the 3-D internal mode computations. The bottom friction is expressed in terms of bottom velocity, which is different from the previous works. Besides, the BFCs are supposed to be spatially varying, i.e. the BFCs at some grid points are selected as the independent BFCs, while the BFCs at other grid points can be obtained through linear interpolation. Based on the simulation of M_2 tide in BNYS, twin experiments are carried out to invert the prescribed distributions of model parameters. The parameters inverted are the Fourier coefficients of OBC, the BFC and the vertical eddy viscosity profiles. In these twin experiments, the real topography of BNYS is installed. The experiments discuss the influence of initial guesses, model errors and data number on the inversion. The inversion has obtained satisfactory results and the prescribed distributions have been successfully inverted, which demonstrates the strong ability of the adjoint method. The results indicate that the inversion of BFC is more sensitive to data error than that of OBC and vertical eddy viscosity profiles. Future work will concentrate on the practical application of this model.

APPENDIX A: COMPUTATION OF FORWARD MODEL

A.1. Computation of external mode

In this model, ADI method is used in the discretization of external mode. ADI method results in computational efficiency superior to fully explicit methods because their improved stability allows large time step to be employed. Equations (7)–(9) are discretized as follows.

When the time step is from n to $n+1$, ζ and U are calculated implicitly, and V are calculated explicitly. The finite difference schemes for calculating ζ and U take the form

$$\zeta_{i,j}^{n+1} + \frac{Hx_{i+1/2,j}^{n}\Delta t}{a_j \Delta\lambda} U_{i+1/2,j}^{n+1} - \frac{Hx_{i-1/2,j}^{n}\Delta t}{a_j \Delta\lambda} U_{i-1/2,j}^{n+1}$$

$$= \zeta_{i,j}^{n} - \frac{\Delta t}{a_j \Delta\phi}\left(Hy_{i,j+1/2}^{n} V_{i,j+1/2}^{n} \cos\phi_{j+1/2} - Hy_{i,j-1/2}^{n} V_{i,j-1/2}^{n} \cos\phi_{j-1/2}\right) \quad \text{(A1)}$$

Copyright © 2007 John Wiley & Sons, Ltd.

DOI: 10.1002/fld

$$U^{n+1}_{i+1/2,j}+\frac{g\Delta t}{a_j\Delta\lambda}\zeta^{n+1}_{i+1,j}-\frac{g\Delta t}{a_j\Delta\lambda}\zeta^{n+1}_{i,j}$$
$$=U^{n}_{i+1/2,j}+\Delta t[f_j(V^n_{i,j})^*+A_h\Delta U^n_{i+1/2,j}-Lx_{i+1/2,j}-Rx_{i+1/2,j}] \tag{A2}$$

where $Hx^n_{i+1/2,j}=hx_{i+1/2,j}+(\zeta^n_{i,j}+\zeta^n_{i+1,j})/2$, $Hy^n_{i,j+1/2}=hy_{i,j+1/2}+(\zeta^n_{i,j}+\zeta^n_{i,j+1})/2$, and the symbol '$_*$' stands for the four-point average, i.e.

$$(V^n_{i,j})^*=(V^n_{i,j+1/2}+V^n_{i,j-1/2}+V^n_{i+1,j-1/2}+V^n_{i+1,j+1/2})/4$$

(A1) and (A2) can be written in the more compact matrix form

$$\mathrm{X}_iU^{n+1}_{i-1/2,j}+\Pi_i\zeta^{n+1}_{i,j}+\Gamma_iU^{n+1}_{i+1/2,j}=\Psi_i \tag{A3}$$

$$\mathrm{X}'_i\zeta^{n+1}_{i,j}+\Pi'_iU^{n+1}_{i+1/2,j}+\Gamma'_i\zeta^{n+1}_{i+1,j}=\Psi'_i \tag{A4}$$

where $\mathrm{X}_i=-Hx^n_{i-1/2,j}\Delta t/a_j\Delta\lambda$, $\Pi_i=1$, $\Gamma_i=Hx^n_{i+1/2,j}\Delta t/a_j\Delta\lambda$, $\mathrm{X}'_i=-g\Delta t/a_j\Delta\lambda$, $\Pi'_i=1$, $\Gamma'_i=g\Delta t/a_j\Delta\lambda$ and Ψ_i, Ψ'_i are the right parts of (A1) and (A2), respectively. (A3) and (A4) constitute a tridiagonal system that can be solved efficiently. Having solved it, ζ^{n+1} and U^{n+1} can thus be obtained.

V^{n+1} are solved by the following explicit scheme:

$$V^{n+1}_{i,j+1/2}=V^n_{i,j+1/2}-\frac{g\Delta t}{R\Delta\phi}(\zeta^{n+1}_{i,j+1}-\zeta^{n+1}_{i,j})$$
$$+\Delta t[-Ly_{i,j+1/2}-Ry_{i,j+1/2}-f_j(U^{n+1}_{i,j})^*+A_h\Delta V^n_{i,j+1/2}] \tag{A5}$$

From $n+1$ to $n+2$, ζ and V are calculated implicitly, and U are solved explicitly. The finite difference schemes for calculating ζ and V take the form

$$\zeta^{n+2}_{i,j}+\frac{\Delta t}{a_j\Delta\phi}(Hy^{n+1}_{i,j+1/2}V^{n+2}_{i,j+1/2}\cos\phi_{j+1/2}-Hy^{n+1}_{i,j-1/2}V^{n+2}_{i,j-1/2}\cos\phi_{j-1/2})$$
$$=\zeta^{n+1}_{i,j}-\frac{Hx^{n+1}_{i+1/2,j}\Delta t}{a_j\Delta\lambda}U^{n+1}_{i+1/2,j}-\frac{Hx^{n+1}_{i-1/2,j}\Delta t}{a_j\Delta\lambda}U^{n+1}_{i-1/2,j} \tag{A6}$$

$$V^{n+2}_{i,j+1/2}+\frac{g\Delta t}{R\Delta\phi}\zeta^{n+2}_{i,j+1}-\frac{g\Delta t}{R\Delta\phi}\zeta^{n+2}_{i,j}$$
$$=V^{n+1}_{i,j+1/2}+\Delta t[-Ly_{i,j+1/2}-Ry_{i,j+1/2}-f_j(U^{n+1}_{i,j})^*+A_h\Delta V^{n+1}_{i,j+1/2}] \tag{A7}$$

Or, in matrix notation,

$$B_jV^{n+2}_{i,j-1/2}+\mathrm{K}_j\zeta^{n+2}_{i,j}+O_jV^{n+2}_{i,j+1/2}=\Omega_j \tag{A8}$$

$$B'_j\zeta^{n+2}_{i,j}+\mathrm{K}'_jV^{n+2}_{i,j+1/2}+O'_j\zeta^{n+2}_{i,j+1}=\Omega'_j \tag{A9}$$

Copyright © 2007 John Wiley & Sons, Ltd.

DOI: 10.1002/fld

where

$$B_j = -\frac{\Delta t\, Hy^{n+1}_{i,j-1/2}\cos\phi_{j-1/2}}{a_j\Delta\phi},\quad K_j = 1,\quad O_j = \frac{\Delta t\, Hy^{n+1}_{i,j+1/2}\cos\phi_{j+1/2}}{a_j\Delta\phi}$$

$$B'_j = -\frac{g\Delta t}{R\Delta\phi},\quad K'_j = 1,\quad O'_j = \frac{g\Delta t}{R\Delta\phi}$$

and Ω_j, Ω'_j are the right parts of (A6) and (A7), respectively. Equations (A8) and (A9) form a tridiagonal system that can be solved efficiently. Having solved it, ζ^{n+2} and V^{n+2} can then be obtained.

U^{n+2} are calculated by the following explicit scheme:

$$U^{n+2}_{i+1/2,j} = U^{n+1}_{i+1/2,j} - \frac{g\Delta t}{a_j\Delta\lambda}(\zeta^{n+2}_{i+1,j} - \zeta^{n+2}_{i,j}) + \Delta t[f_j(V^{n+2}_{i,j})^* + A_h\Delta U^{n+1}_{i+1/2,j} - Lx_{i+1/2,j} - Rx_{i+1/2,j}] \tag{A10}$$

It should be noticed that Lx, Ly, Rx and Ry are unchanged from $n = n^* + 1$ to $n = n^* + q$, where $n^* = q \times m$ and m is the index of internal mode. Their expressions will be given in the next section.

A.2. Computation of internal mode

The discretization of internal mode is similar to that of Casulli and Cheng [3], in which the convective, Coriolis and horizontal viscosity terms in the momentum equations were discretized explicitly and the vertical mixing term was discretized implicitly in order to eliminate a stability condition due to the vertical eddy viscosity. Then we can obtain the finite difference schemes of Equations (1)-(3) as follows.

Assuming k is the index of vertical layers, for the surface layer ($k = 1$) the discretization takes the form

$$\left[(\Delta z_{i+1/2,j,1} + \zeta^{m+1/2}_{i,j}) + \frac{\Delta T\,\mathrm{Av}_{i,j,3/2}}{\Delta z_{i+1/2,j,3/2}}\right] u^{m+1}_{i+1/2,j,1} + \left(-\frac{\Delta T\,\mathrm{Av}_{i,j,3/2}}{\Delta z_{i+1/2,j,3/2}}\right) u^{m+1}_{i+1/2,j,2}$$
$$= (\Delta z_{i+1/2,j,1} + \zeta^{m+1/2}_{i,j})\left[Fu^m_{i+1/2,j,1} - \frac{g\Delta T}{a_j\Delta\lambda}(\zeta^{m+1/2}_{i+1,j} - \zeta^{m+1/2}_{i,j})\right] \tag{A11}$$

$$\left[(\Delta z_{i,j+1/2,1} + \zeta^{m+1/2}_{i,j}) + \frac{\Delta T\,\mathrm{Av}_{i,j,3/2}}{\Delta z_{i,j+1/2,3/2}}\right] v^{m+1}_{i,j+1/2,1} + \left(-\frac{\Delta T\,\mathrm{Av}_{i,j,3/2}}{\Delta z_{i,j+1/2,3/2}}\right) v^{m+1}_{i,j+1/2,2}$$
$$= (\Delta z_{i,j+1/2,1} + \zeta^{m+1/2}_{i,j})\left[Fv^m_{i,j+1/2,1} - \frac{g\Delta T}{R\Delta\phi}(\zeta^{m+1/2}_{i,j+1} - \zeta^{m+1/2}_{i,j})\right] \tag{A12}$$

Copyright © 2007 John Wiley & Sons, Ltd.

DOI: 10.1002/fld

For the middle layers ($1<k<Kx$ and $1<k<Ky$),

$$-\frac{\Delta T\,\mathrm{Av}_{i,j,k-1/2}}{\Delta z_{i+1/2,j.k-1/2}}u^{m+1}_{i+1/2,j,k-1}+\left(\Delta z_{i+1/2,j,k}+\frac{\Delta T\,\mathrm{Av}_{i,j,k-1/2}}{\Delta z_{i+1/2,j.k-1/2}}+\frac{\Delta T\,\mathrm{Av}_{i,j,k+1/2}}{\Delta z_{i+1/2,j.k+1/2}}\right)u^{m+1}_{i+1/2,j,k}$$
$$-\frac{\Delta T\,\mathrm{Av}_{i,j,k+1/2}}{\Delta z_{i+1/2,j.k+1/2}}u^{m+1}_{i+1/2,j,k+1}=\Delta z_{i+1/2,j,k}\left[Fu^{m}_{i+1/2,j,k}-\frac{g\Delta T}{a_j\Delta\lambda}(\zeta^{m+1/2}_{i+1,j}-\zeta^{m+1/2}_{i,j})\right] \quad \text{(A13)}$$

$$-\frac{\Delta T\,\mathrm{Av}_{i,j,k-1/2}}{\Delta z_{i,j+1/2,k-1/2}}v^{m+1}_{i,j+1/2,k-1}+(\Delta z_{i,j+1/2,k}+\frac{\Delta T\,\mathrm{Av}_{i,j,k-1/2}}{\Delta z_{i,j+1/2,k-1/2}}+\frac{\Delta T\,\mathrm{Av}_{i,j,k+1/2}}{\Delta z_{i,j+1/2,k+1/2}})v^{m+1}_{i,j+1/2,k}$$
$$-\frac{\Delta T\,\mathrm{Av}_{i,j,k+1/2}}{\Delta z_{i,j+1/2,k+1/2}}v^{m+1}_{i,j+1/2,k+1}=\Delta z_{i,j+1/2,k}\left[Fv^{m}_{i,j+1/2,k}-\frac{g\Delta T}{R\Delta\phi}(\zeta^{m+1/2}_{i,j+1}-\zeta^{m+1/2}_{i,j})\right] \quad \text{(A14)}$$

For the bottom layer ($k=Kx$ and $k=Ky$),

$$-\frac{\Delta T\,\mathrm{Av}_{i,j,Kx-1/2}}{\Delta z_{i+1/2,j,Kx-1/2}}u^{m+1}_{i+1/2,j,Kx-1}+\left(\Delta z_{i+1/2,j,Kx}+\frac{\Delta T\,\mathrm{Av}_{i,j,Kx-1/2}}{\Delta z_{i+1/2,j,Kx-1/2}}\right.$$
$$\left.+\ \Delta T C_d[u^2_{i+1/2,j,Kx}+(v^*_{i,j,Kx})^2]^{1/2}\right)u^{m+1}_{i+1/2,j,Kx}$$
$$=\Delta z_{i+1/2,j,Kx}\left[Fu^{m}_{i+1/2,j,Kx}-\frac{g\Delta T}{a_j\Delta\lambda}(\zeta^{m+1/2}_{i+1,j}-\zeta^{m+1/2}_{i,j})\right] \quad \text{(A15)}$$

$$-\frac{\Delta T\,\mathrm{Av}_{i,j,Ky-1/2}}{\Delta z_{i,j+1/2,Ky-1/2}}v^{m+1}_{i,j+1/2,Ky-1}+\left(\Delta z_{i,j+1/2,Ky}+\frac{\Delta T\,\mathrm{Av}_{i,j+1/2,Ky-1/2}}{\Delta z_{i,j+1/2,Ky-1/2}}\right.$$
$$\left.+\ \Delta T C_d[v^2_{i,j+1/2,Kx}+(u^*_{i,j,Kx})^2]^{1/2}\right)v^{m+1}_{i,j+1/2,Ky}$$
$$=\Delta z_{i,j+1/2,Ky}\left[Fv^{m}_{i,j+1/2,Ky}-\frac{g\Delta T}{R\Delta\phi}(\zeta^{m+1/2}_{i,j+1}-\zeta^{m+1/2}_{i,j})\right] \quad \text{(A16)}$$

Fu and Fv contain the convective, horizontal viscosity and Coriolis terms of Equations (1) and (2) which are discretized explicitly

$$Fu^{m}_{i+1/2,j,k}=u^{m}_{i+1/2,j,k}+\Delta T(-lx^{m}_{i+1/2,j,k}+A_h\Delta u^{m}_{i+1/2,j,k}+2\omega\sin\phi_j(v^{m}_{i,j,k})^*)$$
$$Fv^{m}_{i,j+1/2,k}=v^{m}_{i,j+1/2,k}+\Delta T(-ly^{m}_{i,j+1/2,k}+A_h\Delta v^{m}_{i,j+1/2,k}-2\omega\sin\phi_j(u^{m}_{i,j,k})^*)$$

In detail, the convective terms are discretized using the upwind schemes as follows:

$$lx^{m}_{i+1/2,j,k}=tu1+tu2+tu3-\frac{(v^{m}_{i,j,k})^*u^{m}_{i+1/2,j,k}\tan\phi_j}{R}$$

Copyright © 2007 John Wiley & Sons, Ltd.

DOI: 10.1002/fld

$$ly^m_{i,j+1/2,k}=tv1+tv2+tv3+\frac{(u^m_{i,j,k})^*(u^m_{i,j,k})^*\tan\phi_{j+1/2}}{R}$$

where

$$tu1=\begin{cases}\dfrac{u^m_{i+1/2,j,k}(u^m_{i+1/2,j,k}-u^m_{i+1/2-1,j,k})}{a_j\Delta\lambda}, & u^m_{i+1/2,j,k}\geqslant 0\\ \dfrac{u^m_{i+1/2,j,k}(u^m_{i+1/2+1,j,k}-u^m_{i+1/2,j,k})}{a_j\Delta\lambda}, & u^m_{i+1/2,j,k}<0\end{cases}$$

$$tu2=\begin{cases}\dfrac{(v^m_{i,j,k})^*(u^m_{i+1/2,j,k}-u^m_{i+1/2,j-1,k})}{R\Delta\phi}, & (v^m_{i,j,k})^*\geqslant 0\\ \dfrac{(v^m_{i,j,k})^*(u^m_{i+1/2,j+1,k}-u^m_{i+1/2,j,k})}{R\Delta\phi}, & (v^m_{i,j,k})^*<0\end{cases}$$

$$tu3=\begin{cases}\dfrac{(w^m_{i,j,1-1/2}+w^m_{i+1,j,1-1/2}+w^m_{i,j,1+1/2}+w^m_{i+1,j,1+1/2})(u^m_{i+1/2,j,2}-u^m_{i+1/2,j,1})}{4\Delta z_{i+1/2,j,3/2}},\\ \quad k=1\\ \dfrac{1}{4}\left[\dfrac{(w^m_{i,j,k-1/2}+w^m_{i+1,j,k-1/2})(u^m_{i+1/2,j,k}-u^m_{i+1/2,j,k-1})}{\Delta z_{i+1/2,j,k-1/2}}\right.\\ \quad \left.+\dfrac{(w^m_{i,j,k+1/2}+w^m_{i+1,j,k+1/2})(u^m_{i+1/2,j,k+1}-u^m_{i+1/2,j,k})}{\Delta z_{i+1/2,j,k+1/2}}\right]\\ \quad k=2,3,\ldots,Kx_{i+1/2,j}\end{cases}$$

$$tv1=\begin{cases}\dfrac{(u^m_{i,j,k})^*(v^m_{i,j+1/2,k}-v^m_{i-1,j+1/2,k})}{a_{j+1/2}\Delta\lambda}, & (u^m_{i,j,k})^*\geqslant 0\\ \dfrac{(u^m_{i,j,k})^*(v^m_{i+1,j+1/2,k}-v^m_{i,j+1/2,k})}{a_{j+1/2}\Delta\lambda}, & (u^m_{i,j,k})^*<0\end{cases}$$

$$tv2=\begin{cases}\dfrac{v^m_{i,j+1/2,k}(v^m_{i,j+1/2,k}-v^m_{i,j+1/2-1,k})}{R\Delta\phi}, & v^m_{i,j+1/2,k}\geqslant 0\\ \dfrac{v^m_{i,j+1/2,k}(v^m_{i,j+1/2+1,k}-v^m_{i,j+1/2,k})}{R\Delta\phi}, & v^m_{i,j+1/2,k}<0\end{cases}$$

Copyright © 2007 John Wiley & Sons, Ltd.

DOI: 10.1002/fld

$$tv3=\begin{cases}\dfrac{(w^m_{i,j,1-1/2}+w^m_{i,j+1,1-1/2}+w^m_{i,j,1+1/2}+w^m_{i,j+1,1+1/2})(v^m_{i,j+1/2,2}-v^m_{i,j+1/2,1})}{4\Delta z_{i,j+1/2,3/2}} \\ \quad k=1 \\ \dfrac{1}{4}\left[\dfrac{(w^m_{i,j,k-1/2}+w^m_{i,j+1,k-1/2})(v^m_{i,j+1/2,k}-v^m_{i,j+1/2,k-1})}{\Delta z_{i,j+1/2,k-1/2}}\right. \\ \quad \left.+\dfrac{(w^m_{i,j,k+1/2}+w^m_{i,j+1,k+1/2})(v^m_{i,j+1/2,k+1}-v^m_{i,j+1/2,k})}{\Delta z_{i,j+1/2,k+1/2}}\right] \\ \quad k=2,3,\ldots,Ky_{i,j+1/2}\end{cases}$$

The discretization of horizontal viscosity terms takes the form

$$\Delta u^m_{i+1/2,j}=\frac{u^m_{i+1/2+1,j}-2u^m_{i+1/2,j}+u^m_{i+1/2-1,j}}{(a_j\Delta\lambda)^2}+\frac{(u^m_{i+1/2,j+1}-u^m_{i+1/2,j})\cos\phi_{j+1/2}-(u^m_{i+1/2,j}-u^m_{i+1/2,j-1})\cos\phi_{j-1/2}}{(R\Delta\phi)^2\cos\phi_j}$$

$$\Delta v^m_{i,j+1/2}=\frac{v^m_{i+1,j+1/2}-2v^m_{i,j+1/2}+v^m_{i-1,j+1/2}}{(a_j\Delta\lambda)^2}+\frac{(v^m_{i,j+1/2+1}-v^m_{i,j+1/2})\cos\phi_{j+1/2}-(v^{m`}_{i,j+1/2}-v^m_{i,j+1/2-1})\cos\phi_{j-1/2}}{(R\Delta\phi)^2\cos\phi_j}$$

Schemes (A11)–(A16) can be written in the more compact matrix form, and at u-points the finite difference schemes are given by

$$\begin{aligned}E_1u^{m+1}_{i+1/2,j,1}+T_1u^{m+1}_{i+1/2,j,2}&=F_1(k=1)\\ A_ku^{m+1}_{i+1/2,j,k-1}+E_ku^{m+1}_{i+1/2,j,k}+T_ku^{m+1}_{i+1/2,j,k+1}&=F_k(k=2,3,\ldots,Kx-1)\\ A_{Kx}u^{m+1}_{i+1/2,j,Kx-1}+E_{Kx}u^{m+1}_{i+1/2,j,Kx}&=F_{Kx}(k=Kx)\end{aligned}\tag{A17}$$

At v-points they are given by

$$\begin{aligned}E'_1v^{m+1}_{i,j+1/2,1}+T'_1v^{m+1}_{i,j+1/2,2}&=F'_1(k=1)\\ A'_kv^{m+1}_{i,j+1/2,k-1}+E'_kv^{m+1}_{i,j+1/2,k}+T'_kv^{m+1}_{i,j+1/2,k+1}&=F'_k(k=2,3,\ldots,Ky-1)\\ A'_{Ky}v^{m+1}_{i,j+1/2,Ky-1}+E'_{Ky}v^{m+1}_{i,j+1/2,Ky}&=F'_{Ky}(k=Ky)\end{aligned}\tag{A18}$$

where

$$E_1=(\Delta z_{i+1/2,j,1}+\zeta^{m+1/2}_{i,j})+\frac{\Delta T\,\mathrm{Av}_{i,j,3/2}}{\Delta z_{i+1/2,j,3/2}},\quad T_1=-\frac{\Delta T\,\mathrm{Av}_{i,j,3/2}}{\Delta z_{i+1/2,j,3/2}},\quad A_k=-\frac{\Delta T\,\mathrm{Av}_{i,j,k-1/2}}{\Delta z_{i+1/2,j,k-1/2}}$$

Copyright © 2007 John Wiley & Sons, Ltd.

DOI: 10.1002/fld

$$E_k=\Delta z_{i+1/2,j,k}+\frac{\Delta T\,\mathrm{Av}_{i,j,k-1/2}}{\Delta z_{i+1/2,j,k-1/2}}+\frac{\Delta T\,\mathrm{Av}_{i,j,k+1/2}}{\Delta z_{i+1/2,j,k+1/2}}$$

$$T_k=-\frac{\Delta T\,\mathrm{Av}_{i,j,k+1/2}}{\Delta z_{i+1/2,j,k+1/2}},\quad A_{Kx}=-\frac{\Delta T\,\mathrm{Av}_{i,j,Kx-1/2}}{\Delta z_{i+1/2,j,Kx-1/2}}$$

$$E_{Kx}=\Delta z_{i+1/2,j,Kx}+\frac{\Delta T\,\mathrm{Av}_{i,j,Kx-1/2}}{\Delta z_{i+1/2,j,Kx-1/2}}+\Delta T C_d[u^2_{i+1/2,j,Kx}+(v^*_{i,j,Kx})^2]^{1/2}$$

$$E'_1=(\Delta z_{i,j+1/2,1}+\zeta^{m+1/2}_{i,j})+\frac{\Delta T\,\mathrm{Av}_{i,j,3/2}}{\Delta z_{i,j+1/2,3/2}},\quad T'_1=-\frac{\Delta T\,\mathrm{Av}_{i,j,3/2}}{\Delta z_{i,j+1/2,3/2}},\quad A'_k=-\frac{\Delta T\,\mathrm{Av}_{i,j,k-1/2}}{\Delta z_{i,j+1/2,k-1/2}}$$

$$E'_k=\Delta z_{i,j+1/2,k}+\frac{\Delta T\,\mathrm{Av}_{i,j,k-1/2}}{\Delta z_{i,j+1/2,k-1/2}}+\frac{\Delta T\,\mathrm{Av}_{i,j,k+1/2}}{\Delta z_{i,j+1/2,k+1/2}}$$

$$T'_k=-\frac{\Delta T\,\mathrm{Av}_{i,j,k+1/2}}{\Delta z_{i,j+1/2,k+1/2}},\quad A'_{Ky}=-\frac{\Delta T\,\mathrm{Av}_{i,j,Ky-1/2}}{\Delta z_{i,j+1/2,Ky-1/2}}$$

$$E'_{Ky}=\Delta z_{i,j+1/2,Ky}+\frac{\Delta T\,\mathrm{Av}_{i,j+1/2,Ky-1/2}}{\Delta z_{i,j+1/2,Ky-1/2}}+\Delta T C_d[v^2_{i,j+1/2,Kx}+(u^*_{i,j,Kx})^2]^{1/2}$$

$F_1, F_k, F_{kx}, F'_1, F'_k$ and F'_{ky} equal to the right parts of (A11)–(A16), respectively. Equations (A17) and (A18) are both tridiagonal systems that can be solved efficiently. After that, u^{m+1} and v^{m+1} can be obtained.

Then the model-produced u and v are adjusted to coincide with the U and V of external mode. The adjusting is given by

$$(u^{m+1}_{i+1/2,j,k})'=u^{m+1}_{i+1/2,j,k}+\delta u_{i+1/2,j},\quad (v^{m+1}_{i,j+1/2,k})'=v^{m+1}_{i,j+1/2,k}+\delta u_{i,j+1/2} \tag{A19}$$

where

$$\delta u_{i+1/2,j}=U_{i+1/2,j}-\frac{1}{Hx_{i+1/2,j}}\sum_{k=1}^{Kx}\{[\Delta z_{i+1/2,j,k}+\sigma_k(\zeta_{i,j}+\zeta_{i+1,j})/2]u^{m+1}_{i+1/2,j,k}\}$$

$$\delta v_{i,j+1/2}=V_{i,j+1/2}-\frac{1}{Hy_{i,j+1/2}}\sum_{k=1}^{Ky}\{[\Delta z_{i,j+1/2,k}+\sigma_k(\zeta^+_{i,j}\zeta_{i,j+1})/2]v^{m+1}_{i,j+1/2,k}\}$$

In the following computations, the values used are u' and v'; however, we will still use the expressions u and v for simplicity.

Finally, by discretizing the continuity equation (3), the vertical component of the velocity w at the new time level is given by

$$w^{m+1}_{i,j,k-1/2}=w^{m+1}_{i,j,k+1/2}+\frac{\Delta z_{i+1/2,j,k}+\sigma_k\zeta^{m+1/2}_{i,j}}{a_j}\left(\frac{u^{m+1}_{i+1/2,j,k}-u^{m+1}_{i-1/2,j,k}}{\Delta\lambda}\right.$$
$$\left.-\frac{v^{n+1}_{i,j+1/2,k}\cos\phi_{j+1/2}-v^{n+1}_{i,j-1/2,k}\cos\phi_{j-1/2}}{\Delta\phi}\right)\quad (k=1,2,\ldots,M_{i,j}) \tag{A20}$$

Copyright © 2007 John Wiley & Sons, Ltd.

DOI: 10.1002/fld

Lx, Ly, Rx and Ry in Appendix A.1 are calculated in the internal mode. In detail, Lx and Ly are the depth average of lx and ly, respectively, and their expressions are given by the following formulas:

$$Lx^m_{i+1/2,j,k} = \frac{\sum_{k=1}^{Kx} [lx^m_{i+1/2,j,k}(\Delta z_{i+1/2,j,k} + \sigma_k \zeta_{i,j})]}{Hx_{i+1/2,j}}$$

$$Ly^m_{i,j+1/2,k} = \frac{\sum_{k=1}^{Ky} [ly^m_{i,j+1/2,k}(\Delta z_{i,j+1/2,k} + \sigma_k \zeta_{i,j})]}{Hy_{i,j+1/2}}$$

In the previous works on the 3-D adjoint tidal model [20, 21], the bottom friction is expressed in terms of depth-integrated velocities. However, for the bottom friction, turbulent boundary layer models of the near-bottom flow indicate that it is physically realistic to use a quadratic dependence of bottom friction on the bottom velocity. Therefore, the bottom friction is expressed in terms of bottom velocity in our model. For internal mode, the bottom friction is given by (6) and has the form

$$R'x_{i+1/2,j} = C_d[u^2_{i+1/2,j,Kx} + (v^*_{i,j,Kx})^2]^{1/2} u_{i+1/2,j,Kx}$$

$$R'y_{i,j+1/2} = C_d[v^2_{i,j+1/2,Ky} + (u^*_{i,j,Ky})^2]^{1/2} v_{i,j+1/2,Ky}$$

In the external mode, the bottom friction is the depth average of $R'x$ and $R'y$ and has the following expression:

$$Rx_{i+1/2,j} = \frac{Rx'_{i+1/2,j}}{Hx_{i+1/2,j}}, \quad Ry_{i,j+1/2} = \frac{Ry'_{i,j+1/2}}{Hy_{i,j+1/2}}$$

APPENDIX B: DERIVATION OF ADJOINT MODEL

B.1. External mode of adjoint model

In AE, β, τ, δ are calculated by

$$\frac{\partial L}{\partial \zeta} = 0, \quad \frac{\partial L}{\partial U} = 0, \quad \frac{\partial L}{\partial V} = 0 \tag{B1}$$

ADI method is also employed to solve Equations (B1) and the computation process is similar to that of FE in Appendix A1.

When the time step is from $n+1$ to n, β and τ are calculated implicitly, and δ are calculated explicitly. The finite difference schemes for calculating β and τ take the form

$$\frac{g\Delta t}{a_j \Delta\lambda}\tau^n_{i-1/2,j} + \beta^n_{i,j} - \frac{g\Delta t}{a_j \Delta\lambda}\tau^n_{i+1/2,j}$$

$$= \beta^{n+1}_{i,j} - \Delta t K_\zeta D_{i,j}(\zeta^n_{i,j} - \hat{\zeta}^n_{i,j}) + \frac{g\Delta t}{R\Delta\phi}(\delta^{n+1}_{i,j+1/2} - \delta^{n+1}_{i,j-1/2}) + Y_{i,j} \tag{B2}$$

Copyright © 2007 John Wiley & Sons, Ltd.

DOI: 10.1002/fld

$$\frac{H^n_{i,j}\Delta t}{a_j\Delta\lambda}\beta^n_{i,j}+\tau^n_{i+1/2,j}-\frac{H^n_{i+1,j}\Delta t}{a_j\Delta\lambda}\beta^n_{i+1,j}$$
$$=\tau^{n+1}_{i+1/2,j}+\Delta t[-f_j(\delta^{n+1}_{i,j})^*+A_h\Delta\tau^{n+1}_{i+1/2,j}-aLx_{i+1/2,j}-aRx_{i+1/2,j}] \tag{B3}$$

(B2) and (B3) can be rewritten in the matrix form as

$$X_i\tau^n_{i-1/2,j}+\Pi_i\beta^n_{i,j}+\Gamma_i\tau^n_{i+1/2,j}=\Psi_i \tag{B4}$$
$$X'_i\beta^n_{i,j}+\Pi'_i\tau^n_{i+1/2,j}+\Gamma'_i\beta^n_{i+1,j}=\Psi'_i \tag{B5}$$

where $X_i=g\Delta t/a_j\Delta\lambda, \Pi_i=1, \Gamma_i=-g\Delta t/a_j\Delta\lambda, X'_i=H^n_{i,j}\Delta t/a_j\Delta\lambda, \Pi'_i=1, \Gamma'_i=-H^n_{i+1,j}\Delta t/a_j\Delta\lambda$, and Ψ_i, Ψ'_i equal to the right sides of (B2) and (B3), respectively. τ^n and β^n can be obtained by solving the tridiagonal systems of (B4) and (B5).

δ^n are calculated by the following explicit scheme:

$$\delta^n_{i,j+1/2}=\delta^{n+1}_{i,j+1/2}+\frac{\Delta t}{a_j\Delta\phi}(H^n_{i,j+1}\beta^{n+1}_{i,j+1}\cos\phi_{j+1/2}-H^n_{i,j}\beta^{n+1}_{i,j}\cos\phi_{j-1/2})$$
$$+\Delta t[f_j(\tau^{n+1}_{i,j})^*+A_h\Delta\delta^{n+1}_{i,j+1/2}-aLy_{i,j+1/2}-aRy_{i,j+1/2}] \tag{B6}$$

From n to $n-1$, β and δ are calculated implicitly, and τ are calculated explicitly. The finite difference schemes for calculating β, δ are given by

$$\frac{g\Delta t}{R\Delta\phi}\delta^{n-1}_{i,j-1/2}+\beta^{n-1}_{i,j}-\frac{g\Delta t}{R\Delta\phi}\delta^{n-1}_{i,j+1/2}$$
$$=\beta^n_{i,j}-\Delta t K_\zeta D_{i,j}(\zeta^{n-1}_{i,j}-\hat{\zeta}^{n-1}_{i,j})+\frac{g\Delta t}{a_j\Delta\lambda}(\tau^n_{i+1/2,j}-\tau^n_{i-1/2,j})+Y_{i,j} \tag{B7}$$
$$\frac{H^{n-1}_{i,j}\cos\phi_{j-1/2}\Delta t}{a_j\Delta\phi}\beta^{n-1}_{i,j}+\delta^{n-1}_{i,j+1/2}-\frac{H^{n-1}_{i,j+1}\cos\phi_{j+1/2}\Delta t}{a_j\Delta\phi}\beta^{n-1}_{i,j+1}$$
$$=\delta^n_{i,j+1/2}+\Delta t[f_j(\tau^n_{i,j})^*+A_h\Delta\delta^n_{i,j+1/2}-aLy_{i,j+1/2}-aRy_{i,j+1/2}] \tag{B8}$$

The matrix notation of (B7) and (B8) is given by

$$B_j\delta^{n-1}_{i,j-1/2}+K_j\beta^{n-1}_{i,j}+O_j\delta^{n-1}_{i,j+1/2}=\Omega_j \tag{B9}$$
$$B'_j\beta^{n-1}_{i,j}+K'_j\delta^{n-1}_{i,j+1/2}+O'_j\beta^{n-1}_{i,j+1}=\Omega'_j \tag{B10}$$

where $B_j=g\Delta t/R\Delta\phi, K_j=1, O_j=-g\Delta t/R\Delta\phi$, $B'_j=H^{n-1}_{i,j}\cos\phi_{j-1/2}\Delta t/a_j\Delta\phi, K'_j=1, O'_j=-H^{n-1}_{i,j+1}\cos\phi_{j+1/2}\Delta t/a_j\Delta\phi$, and Ω_j, Ω'_j equal to the right parts of (B7) and (B8), respectively.

Copyright © 2007 John Wiley & Sons, Ltd.

DOI: 10.1002/fld

Equations (B9) and (B10) constitute a tridiagonal system that can be easily solved. Having solved it, β^{n-1} and δ^{n-1} can then be obtained.

τ^{n-1} are solved by the following explicit scheme:

$$\tau^{n-1}_{i+1/2,j} = \tau^{n}_{i+1/2,j} + \frac{\Delta t}{a_j \Delta\lambda}(H^{n-1}_{i+1,j}\beta^{n}_{i+1,j} - H^{n-1}_{i,j}\beta^{n}_{i,j}) + \Delta t[-f_j(\delta^{n}_{i,j})^* + A_h \Delta\tau^{n+1}_{i+1/2,j} - aLx_{i+1/2,j} - aRx_{i+1/2,j}] \tag{B11}$$

$Y_{i,j}, aLx_{i+1/2,j}, aLy_{i,j+1/2,}, aRx_{i+1/2,j}, aRy_{i,j+1/2}$ of Equations (B2)–(B11) that are calculated in AI will keep unchanged from $n=n'+q, n'+q-1, \ldots, n'+1$ ($n'=q\times m$), and their expressions will be given in the next section.

B.2. Internal mode of adjoint model

The numerical schemes of AI are given by

$$\frac{\partial L}{\partial u}=0, \quad \frac{\partial L}{\partial v}=0 \tag{B12}$$

where μ and γ are calculated. We also assume that k is the index of vertical layers. For the surface layer ($k=1$), the discretization takes the form

$$\left[(\Delta z_{i+1/2,j,1}+\zeta^{m+1/2}_{i,j}) + \frac{\Delta T \mathrm{Av}_{i,j,3/2}}{\Delta z_{i+1/2,j,3/2}}\right]\mu^{m}_{i+1/2,j,1} + \left(-\frac{\Delta T \mathrm{Av}_{i,j,3/2}}{\Delta z_{i+1/2,j,3/2}}\right)\mu^{m}_{i+1/2,j,2}$$
$$= (\Delta z_{i+1/2,j,1}+\zeta^{m+1/2}_{i,j})\mu^{m+1}_{i+1/2,j,1} - (\Delta z_{i+1/2,j,1}+\zeta^{m+1/2}_{i,j})\Delta T[alx^{m+1}_{i+1/2,j,1} + f_j(\gamma^{m+1}_{i,j,1})^*$$
$$- A_h\Delta\mu^{m+1}_{i+1/2,j,1} + K_u D'_{i+1/2,j,1}(u^{m}_{i+1/2,j,1} - \hat{u}^{m}_{i+1/2,j,1}) + zx^{m+1/2}_{i+1/2,j,1}] \tag{B13}$$

$$\left[(\Delta z_{i,j+1/2,1}+\zeta^{m+1/2}_{i,j}) + \frac{\Delta T \mathrm{Av}_{i,j,3/2}}{\Delta z_{i,j+1/2,3/2}}\right]\gamma^{m}_{i+1/2,j,1} + \left(-\frac{\Delta T \mathrm{Av}_{i,j,3/2}}{\Delta z_{i,j+1/2,3/2}}\right)\gamma^{m}_{i+1/2,j,2}$$
$$= (\Delta z_{i,j+1/2,1}+\zeta^{m+1/2}_{i,j})\gamma^{m+1}_{i,j+1/2,1} - (\Delta z_{i,j+1/2,1}+\zeta^{m+1/2}_{i,j})\Delta T[aly^{m+1}_{i,j+1/2,1} - f_j(\mu^{m+1}_{i,j,1})^*$$
$$- A_h\Delta\gamma^{m+1}_{i,j+1/2,1} + K_v D'_{i,j+1/2,1}(v^{m}_{i,j+1/2,1} - \hat{v}^{m}_{i,j+1/2,1}) + zy^{m+1/2}_{i,j+1/2,1}] \tag{B14}$$

For the middle layers ($1<k<Kx$ and $1<k<Ky$),

$$\left(-\frac{\Delta T \mathrm{Av}_{i,j,k-1/2}}{\Delta z_{i+1/2,j,k-1/2}}\right)\mu^{m}_{i+1/2,j,k-1} + \left(\Delta z_{i+1/2,j,k} + \frac{\Delta T \mathrm{Av}_{i,j,k-1/2}}{\Delta z_{i+1/2,j,k-1/2}} + \frac{\Delta T \mathrm{Av}_{i,j,k+1/2}}{\Delta z_{i+1/2,j,k+1/2}}\right)\mu^{m}_{i+1/2,j,k}$$
$$+ \left(-\frac{\Delta T \mathrm{Av}_{i,j,k+1/2}}{\Delta z_{i+1/2,j,k+1/2}}\right)\mu^{m}_{i+1/2,j,k+1}$$

Copyright © 2007 John Wiley & Sons, Ltd.

DOI: 10.1002/fld

$$
\begin{aligned}
&= \Delta z_{i+1/2,j,k}\mu^{m+1}_{i+1/2,j,k} - \Delta z_{i+1/2,j,k}\Delta T[alx^{m+1}_{i+1/2,j,k} \\
&\quad + f_j(\gamma^{m+1}_{i,j,k})^* - A_h\Delta\mu^{m+1}_{i+1/2,j,k} + K_u D'_{i+1/2,j,k}(u^m_{i+1/2,j,k} - \hat{u}^m_{i+1/2,j,k}) + zx^{m+1/2}_{i+1/2,j,k}] \qquad \text{(B15)}
\end{aligned}
$$

$$
\begin{aligned}
&\left(-\frac{\Delta T\,\mathrm{Av}_{i,j,k-1/2}}{\Delta z_{i,j+1/2,k-1/2}}\right)\gamma^m_{i,j+1/2,k-1} + \left(\Delta z_{i,j+1/2,k} + \frac{\Delta T\,\mathrm{Av}_{i,j,k-1/2}}{\Delta z_{i,j+1/2,k-1/2}} + \frac{\Delta T\,\mathrm{Av}_{i,j,k+1/2}}{\Delta z_{i,j+1/2,k+1/2}}\right)\gamma^m_{i,j+1/2,k} \\
&\quad + \left(-\frac{\Delta T\,\mathrm{Av}_{i,j,k+1/2}}{\Delta z_{i,j+1/2,k+1/2}}\right)\gamma^m_{i,j+1/2,k+1} \\
&= \Delta z_{i,j+1/2,k}\gamma^{m+1}_{i+1/2,j,k} - \Delta z_{i,j+1/2,k}\Delta T[aly^{m+1}_{i,j+1/2,k} \\
&\quad - f_j(\mu^{m+1}_{i,j,k})^* - A_h\Delta\gamma^{m+1}_{i,j+1/2,k} + K_v D'_{i,j+1/2,k}(v^m_{i,j+1/2,k} - \hat{v}^m_{i,j+1/2,k}) + zy^{m+1/2}_{i,j+1/2,k}] \qquad \text{(B16)}
\end{aligned}
$$

For the bottom layer ($k = Kx$ and $k = Ky$),

$$
\begin{aligned}
&\left(-\frac{\Delta T\,\mathrm{Av}_{i,j,Kx-1/2}}{\Delta z_{i+1/2,j,Kx-1/2}}\right)\mu^m_{i+1/2,j,Kx-1} + \left\{\Delta z_{i+1/2,j,Kx} + \frac{\Delta T\,\mathrm{Av}_{i,j,Kx-1/2}}{\Delta z_{i+1/2,j,Kx-1/2}} + \Delta TC_d[(u^{m-1}_{i+1/2,j,Kx})^2\right. \\
&\quad \left. + ((v^{m-1}_{i,j,Kx})^*)^2]^{1/2}\right\}\mu^m_{i+1/2,j,Kx} \\
&= \Delta z_{i+1/2,j,Kx}\mu^{m+1}_{i+1/2,j,Kx} - \frac{\Delta TC_d u^m_{i+1/2,j,Kx}u^{m+1}_{i+1/2,j,Kx}\mu^{m+1}_{i+1/2,j,Kx}}{[(u^m_{i+1/2,j,Kx})^2 + ((v^m_{i,j,Kx})^*)^2]^{1/2}} \\
&\quad - \Delta z_{i+1/2,j,Kx}\Delta T[alx^{m+1}_{i+1/2,j,Kx} + f_j(\gamma^{m+1}_{i,j,Kx})^* \\
&\quad - A_h\Delta\mu^{m+1}_{i+1/2,j,Kx} + K_u D'_{i+1/2,j,Kx}(u^m_{i+1/2,j,Kx} - \hat{u}^m_{i+1/2,j,Kx}) + zx^{m+1/2}_{i+1/2,j,Kx}] \qquad \text{(B17)}
\end{aligned}
$$

$$
\begin{aligned}
&\left(-\frac{\Delta T\,\mathrm{Av}_{i,j,Ky-1/2}}{\Delta z_{i,j+1/2,Ky-1/2}}\right)\gamma^m_{i,j+1/2,Ky-1} + \left\{\Delta z_{i,j+1/2,Ky} + \frac{\Delta T\,\mathrm{Av}_{i,j,Ky-1/2}}{\Delta z_{i,j+1/2,Ky-1/2}} + \Delta TC_d[(v^{m-1}_{i,j+1/2,Ky})^2\right. \\
&\quad \left. + ((u^{m-1}_{i,j,Ky})^*)^2]^{1/2}\right\}\gamma^m_{i,j+1/2,Ky} \\
&= \Delta z_{i,j+1/2,Ky}\gamma^{m+1}_{i,j+1/2,Ky} - \frac{\Delta TC_d v^m_{i,j+1/2,Ky}v^{m+1}_{i,j+1/2,Ky}\gamma^{m+1}_{i,j+1/2,Ky}}{[(v^m_{i,j+1/2,Ky})^2 + ((u^m_{i,j,Ky})^*)^2]^{1/2}} \\
&\quad - \Delta z_{i,j+1/2,Ky}\Delta T[aly^{m+1}_{i,j+1/2,Ky} - f_j(\mu^{m+1}_{i,j,Ky})^* \\
&\quad - A_h\Delta\gamma^{m+1}_{i,j+1/2,Ky} + K_v D'_{i,j+1/2,Ky}(v^m_{i,j+1/2,Ky} - \hat{v}^m_{i,j+1/2,Ky}) + zy^{m+1/2}_{i,j+1/2,Ky}] \qquad \text{(B18)}
\end{aligned}
$$

Copyright © 2007 John Wiley & Sons, Ltd.

DOI: 10.1002/fld

zx and zy of Equations (B13)–(B18) are the terms related to AE and can be written in a different form as

$$zx^{m+1}_{i+1/2,j,k}=\begin{cases}\dfrac{\Delta z_{i+1/2,j,k}}{Hx_{i+1/2,j}}(zu_1+zu_2+zu_3)\\ \quad+\dfrac{\Delta z_{i,j+1/2,k}}{Hy_{i,j+1/2}}(zu_4+zu_5), & (k=1,2,3,\ldots,Kx-1)\\ \dfrac{\Delta z_{i+1/2,j,k}}{Hx_{i+1/2,j}}(zu_1+zu_2+zu_3)\\ \quad+\dfrac{\Delta z_{i,j+1/2,k}}{Hy_{i,j+1/2}}(zu_4+zu_5)+zu_6, & (k=Kx)\end{cases}$$

$$zy^{m+1/2}_{i,j+1/2,k}=\begin{cases}\dfrac{\Delta z_{i,j+1/2,k}}{Hy_{i,j+1/2}}(zv_1+zv_2)+\dfrac{\Delta z_{i+1/2,j,k}}{Hx_{i+1/2,j}}(zv_3+zv_4), & k=1,2,3,\ldots,Ky-1\\ \dfrac{\Delta z_{i,j+1/2,k}}{Hy_{i,j+1/2}}(zv_1+zv_2)+\dfrac{\Delta z_{i+1/2,j,k}}{Hx_{i+1/2,j}}(zv_3+zv_4)+zv_5, & k=Ky\end{cases}$$

where

$$zu_1=\begin{cases}\dfrac{\tau^{m+1/2}_{i+1/2,j}(u^m_{i+1/2,j,k}-u^m_{i+1/2-1,j,k})}{a_j\Delta\lambda}\\ \quad-\dfrac{u^m_{i+1/2+1,j,k}\tau^{m+1/2}_{i+1/2+1,j}-u^m_{i+1/2,j,k}\tau^{m+1/2}_{i+1/2,j}}{a_j\Delta\lambda}, & u^m_{i+1/2,j,k}\geqslant 0\\ \dfrac{\tau^{m+1/2}_{i+1/2,j}(u^m_{i+1/2+1,j,k}-u^m_{i+1/2,j,k})}{a_j\Delta\lambda}\\ \quad-\dfrac{u^m_{i+1/2,j,k}\tau^{m+1/2}_{i+1/2,j}-u^m_{i+1/2-1,j,k}\tau^{m+1/2}_{i+1/2-1,j}}{a_j\Delta\lambda}, & u^m_{i+1/2,j,k}<0\end{cases}$$

$$zu_2=\begin{cases}-\dfrac{(v^m_{i,j+1,k})^*\tau^{m+1/2}_{i+1/2,j+1}-(v^m_{i,j,k})^*\tau^{m+1/2}_{i+1/2,j}}{R\Delta\phi}, & (v^m_{i,j,k})^*\geqslant 0\\ -\dfrac{(v^m_{i,j,k})^*\tau^{m+1/2}_{i+1/2,j}-(v^m_{i,j-1,k})^*\tau^{m+1/2}_{i+1/2,j-1}}{R\Delta\phi}, & (v^m_{i,j,k})^*<0\end{cases}$$

$$zu_3=\frac{2(\delta^{m+1/2}_{i,j})^*u^m_{i+1/2,j,k}\tan\phi_{j+1/2}}{R},\quad zu_4=-\frac{\tau^{m+1/2}_{i+1/2,j}(v^m_{i,j,k})^*\tan\phi_j}{R}$$

$$zu_5=\begin{cases}\dfrac{(\delta^{m+1/2}_{i,j})^*[(v^m_{i,j,k})^*-(v^m_{i-1,j,k})^*]}{a_j\Delta\lambda}, & (u^m_{i,j,k})^*\geqslant 0\\ \dfrac{(\delta^{m+1/2}_{i,j})^*[(v^m_{i+1,j,k})^*-(v^m_{i,j,k})^*]}{a_j\Delta\lambda}, & (u^m_{i,j,k})^*<0\end{cases}$$

Copyright © 2007 John Wiley & Sons, Ltd.

DOI: 10.1002/fld

$$zu_6=\frac{\tau^{m+1/2}_{i+1/2,j}C_d}{Hx_{i+1/2,j}}\left\{[(u^m_{i+1/2,j,Kx})^2+((v^m_{i,j,Kx})^*)^2]^{1/2}+\frac{u^m_{i+1/2,j,Kx}u^m_{i+1/2,j,Kx}}{[(u^m_{i+1/2,j,Kx})^2+((v^m_{i,j,Kx})^*)^2]^{1/2}}\right\}$$

$$zv_1=\begin{cases}-\dfrac{(u^m_{i+1,j,k})^*\delta^{m+1/2}_{i+1,j+1/2}-(u^m_{i,j,k})^*\delta^{m+1/2}_{i,j+1/2}}{a_j\Delta\lambda}, & (u^m_{i,j,k})^*\geqslant 0\\ -\dfrac{(u^m_{i,j,k})^*\delta^{m+1/2}_{i,j+1/2}-(u^m_{i-1,j,k})^*\delta^{m+1/2}_{i-1,j+1/2}}{a_j\Delta\lambda}, & (u^m_{i,j,k})^*<0\end{cases}$$

$$zv_2=\begin{cases}\dfrac{\delta^{m+1/2}_{i,j+1/2}(v^m_{i,j+1/2,k}-v^m_{i,j+1/2-1,k})}{R\Delta\phi}\\ \quad -\dfrac{v^m_{i,j+1/2+1,k}\delta^{m+1/2}_{i,j+1/2+1}-v^m_{i,j+1/2,k}\delta^{m+1/2}_{i,j+1/2}}{R\Delta\phi}, & v^m_{i,j+1/2,k}\geqslant 0\\ \dfrac{\delta^{m+1/2}_{i,j+1/2}(v^m_{i,j+1/2+1,k}-v^m_{i,j+1/2,k})}{R\Delta\phi}\\ \quad -\dfrac{v^m_{i,j+1/2,k}\delta^{m+1/2}_{i,j+1/2}-v^m_{i,j+1/2-1,k}\delta^{m+1/2}_{i,j+1/2-1}}{R\Delta\phi}, & v^m_{i,j+1/2,k}<0\end{cases}$$

$$zv_3=-\frac{(\tau^{m+1/2}_{i,j})^*(u^m_{i,j,k})^*\tan\phi_j}{R},\quad zv_4=\begin{cases}\dfrac{(\tau^{m+1/2}_{i,j})^*[(u^m_{i,j,k})^*-(u^m_{i,j-1,k})^*]}{R\Delta\phi}, & (v^m_{i,j,k})^*\geqslant 0\\ \dfrac{(\tau^{m+1/2}_{i,j})^*[(u^m_{i,j+1,k})^*-(u^m_{i,j,k})^*]}{R\Delta\phi}, & (v^m_{i,j,k})^*<0\end{cases}$$

$$zv_5=\frac{\delta^{m+1/2}_{i,j+1/2}C_d}{Hy_{i,j+1/2}}\left\{[(v^m_{i,j+1/2,Ky})^2+((u^m_{i,j,Ky})^*)^2]^{1/2}+\frac{v^m_{i,j+1/2,Ky}v^m_{i,j+1/2,Ky}}{[(v^m_{i+1/2,j,Ky})^2+((u^m_{i,j,Ky})^*)^2]^{1/2}}\right\}$$

$alx_{i+1/2,j,k}$ and $aly_{i,j+1/2,k}$ are the adjoint of convective terms in FI and we discretize them as follows:

$$alx^{m+1}_{i+1/2,j,k}=atu_1+atu_2+atu_3+atu_4+\frac{2(\gamma^{m+1}_{i,j,k})^*u^m_{i+1/2,j,k}\tan\phi_{j+1/2}-\mu^{m+1}_{i+1/2,j,k}(v^m_{i,j,k})^*\tan\phi_j}{R}$$

$$aly^{m+1}_{i,j+1/2,k}=atv_1+atv_2+atv_3+atv_4-\frac{(\mu^{m+1}_{i,j,k})^*(u^m_{i,j,k})^*\tan\phi_j}{R}$$

Copyright © 2007 John Wiley & Sons, Ltd.

DOI: 10.1002/fld

where

$$atu_1=\begin{cases}\dfrac{\mu^{m+1}_{i+1/2,j,k}(u^m_{i+1/2,j,k}-u^m_{i+1/2-1,j,k})}{a_j\Delta\lambda} & \\ \quad -\dfrac{u^m_{i+1/2+1,j,k}\mu^{m+1}_{i+1/2+1,j,k}-u^m_{i+1/2,j,k}\mu^{m+1}_{i+1/2,j,k}}{a_j\Delta\lambda}, & u^m_{i+1/2,j,k}\geqslant 0\\ \dfrac{\mu^{m+1}_{i+1/2,j,k}(u^m_{i+1/2+1,j,k}-u^m_{i+1/2,j,k})}{a_j\Delta\lambda} & \\ \quad -\dfrac{u^m_{i+1/2,j,k}\mu^{m+1}_{i+1/2,j,k}-u^m_{i+1/2-1,j,k}\mu^{m+1}_{i+1/2-1,j,k}}{a_j\Delta\lambda}, & u^m_{i+1/2,j,k}<0\end{cases}$$

$$atu_2=\begin{cases}-\dfrac{(v^m_{i,j+1,k})^*\mu^{m+1}_{i+1/2,j+1,k}-(v^m_{i,j,k})^*\mu^{m+1}_{i+1/2,j,k}}{R\Delta\phi}, & (v^m_{i,j,k})^*\geqslant 0\\ -\dfrac{(v^m_{i,j,k})^*\mu^{m+1}_{i+1/2,j,k}-(v^m_{i,j-1,k})^*\mu^{m+1}_{i+1/2,j-1,k}}{R\Delta\phi}, & (v^m_{i,j,k})^*<0\end{cases}$$

$$atu_4=\begin{cases}\dfrac{(\gamma^{m+1}_{i,j,k})^*[(v^m_{i,j,k})^*-(v^m_{i-1,j,k})^*]}{a_j\Delta\lambda}, & (u^m_{i,j,k})^*\geqslant 0\\ \dfrac{(\gamma^{m+1}_{i,j,k})^*[(v^m_{i+1,j,k})^*-(v^m_{i,j,k})^*]}{a_j\Delta\lambda}, & (u^m_{i,j,k})^*<0\end{cases}$$

$$atu_3=\begin{cases}\dfrac{(w^m_{i,j,1-1/2}+w^m_{i+1,j,1-1/2}+w^m_{i,j,1+1/2}+w^m_{i+1,j,1+1/2})(\mu^{m+1}_{i+1/2,j,2}-\mu^{m+1}_{i+1/2,j,1})}{4\Delta z_{i+1/2,j,3/2}}, & k=1\\ \dfrac{1}{4}\left[\dfrac{(w^m_{i,j,k-1/2}+w^m_{i+1,j,k-1/2})(\mu^{m+1}_{i+1/2,j,k}-\mu^{m+1}_{i+1/2,j,k-1})}{\Delta z_{i+1/2,j,k-1/2}}\right. & \\ \quad \left.+\dfrac{(w^m_{i,j,k+1/2}+w^m_{i+1,j,k+1/2})(\mu^{m+1}_{i+1/2,j,k+1}-\mu^{m+1}_{i+1/2,j,k})}{\Delta z_{i+1/2,j,k+1/2}}\right], & k=2,3,\ldots,Kx\end{cases}$$

$$atv_1=\begin{cases}-\dfrac{(u^m_{i+1,j,k})^*\gamma^{m+1}_{i+1,j+1/2,k}-(u^m_{i,j,k})^*\gamma^{m+1}_{i,j+1/2,k}}{a_j\Delta\lambda}, & (u^m_{i,j,k})^*\geqslant 0\\ -\dfrac{(u^m_{i,j,k})^*\gamma^{m+1}_{i,j+1/2,k}-(u^m_{i-1,j,k})^*\gamma^{m+1}_{i-1,j+1/2,k}}{a_j\Delta\lambda}, & (u^m_{i,j,k})^*<0\end{cases}$$

$$atv_4=\begin{cases}\dfrac{(\mu^{m+1}_{i,j,k})^*[(u^m_{i,j,k})^*-(u^m_{i,j-1,k})^*]}{R\Delta\phi}, & (v^m_{i,j,k})^*\geqslant 0\\ \dfrac{(\mu^{m+1}_{i,j,k})^*[(u^m_{i,j+1,k})^*-(u^m_{i,j,k})^*]}{R\Delta\phi}, & (v^m_{i,j,k})^*<0\end{cases}$$

Copyright © 2007 John Wiley & Sons, Ltd.

DOI: 10.1002/fld

$$atv_2 = \begin{cases} \dfrac{\gamma^{m+1}_{i,j+1/2,k}(v^m_{i,j+1/2,k} - v^m_{i,j+1/2-1,k})}{R\Delta\phi} \\ \quad - \dfrac{v^m_{i,j+1/2+1,k}\gamma^{m+1}_{i,j+1/2+1,k} - v^m_{i,j+1/2,k}\gamma^{m+1}_{i,j+1/2,k}}{R\Delta\phi}, \quad v^m_{i,j+1/2,k} \geqslant 0 \\ \dfrac{\gamma^{m+1}_{i,j+1/2,k}(v^m_{i,j+1/2+1,k} - v^m_{i,j+1/2,k})}{R\Delta\phi} \\ \quad - \dfrac{v^m_{i,j+1/2,k}\gamma^{m+1}_{i,j+1/2,k} - v^m_{i,j+1/2-1,k}\gamma^{m+1}_{i,j+1/2-1,k}}{R\Delta\phi}, \quad v^m_{i,j+1/2,k} < 0 \end{cases}$$

$$atv_3 = \begin{cases} \dfrac{(w^m_{i,j,1-1/2} + w^m_{i,j+1,1-1/2} + w^m_{i,j,1+1/2} + w^m_{i,j+1,1+1/2})(\gamma^{m+1}_{i,j+1/2,2} - \gamma^{m+1}_{i,j+1/2,1})}{4\Delta z_{i,j+1/2,3/2}}, \quad k = 1 \\ \dfrac{1}{4}\left[\dfrac{(w^m_{i,j,k-1/2} + w^m_{i,j+1,k-1/2})(\gamma^{m+1}_{i,j+1/2,k} - \gamma^{m+1}_{i,j+1/2,k-1})}{\Delta z_{i,j+1/2,k-1/2}} \right. \\ \quad \left. + \dfrac{(w^m_{i,j,k+1/2} + w^m_{i,j+1,k+1/2})(\gamma^{m+1}_{i,j+1/2,k+1} - \gamma^{m+1}_{i,j+1/2,k})}{\Delta z_{i,j+1/2,k+1/2}} \right], \quad k = 2, 3, \ldots, Ky \end{cases}$$

Schemes (B13)–(B18) can be written in the more compact matrix form, and at u-points the finite difference schemes are given by

$$\begin{gathered} E_1\mu^m_{i+1/2,j,1} + T_1\mu^m_{i+1/2,j,2} = F_1 \quad (k=1) \\ A_k\mu^m_{i+1/2,j,k-1} + E_k\mu^m_{i+1/2,j,k} + T_k\mu^m_{i+1/2,j,k+1} = F_k \quad (k = 2, 3, \ldots, Kx-1) \\ A_{Kx}\mu^m_{i+1/2,j,Kx-1} + E_{Kx}\mu^m_{i+1/2,j,Kx} = F_{Kx} \quad (k = Kx) \end{gathered} \tag{B19}$$

At v-points they are given by

$$\begin{gathered} E'_1\gamma^m_{i,j+1/2,1} + T'_1\gamma^m_{i,j+1/2,2} = F'_1 \quad (k=1) \\ A'_k\gamma^m_{i,j+1/2,k-1} + E'_k\gamma^m_{i,j+1/2,k} + T'_k\gamma^m_{i,j+1/2,k+1} = F'_k \quad (k = 2, 3, \ldots, Ky-1) \\ A'_{Ky}\gamma^m_{i,j+1/2,Ky-1} + E'_{Ky}\gamma^m_{i,j+1/2,Ky} = F'_{Kx} \quad (k = Ky) \end{gathered} \tag{B20}$$

where

$$E_1 = (\Delta z_{i+1/2,j,1} + \zeta^{m+1/2}_{i,j}) + \frac{\Delta T\,\mathrm{Av}_{i,j,3/2}}{\Delta z_{i+1/2,j,3/2}}, \quad T_1 = -\frac{\Delta T\,\mathrm{Av}_{i,j,3/2}}{\Delta z_{i+1/2,j,3/2}}, \quad A_k = -\frac{\Delta T\,\mathrm{Av}_{i,j,k-1/2}}{\Delta z_{i+1/2,j,k-1/2}}$$

$$E_k = \Delta z_{i+1/2,j,k} + \frac{\Delta T\,\mathrm{Av}_{i,j,k-1/2}}{\Delta z_{i+1/2,j,k-1/2}} + \frac{\Delta T\,\mathrm{Av}_{i,j,k+1/2}}{\Delta z_{i+1/2,j,k+1/2}}$$

$$T_k = -\frac{\Delta T\,\mathrm{Av}_{i,j,k+1/2}}{\Delta z_{i+1/2,j,k+1/2}}, \quad A_{Kx} = -\frac{\Delta T\,\mathrm{Av}_{i,j,Kx-1/2}}{\Delta z_{i+1/2,j,Kx-1/2}}$$

Copyright © 2007 John Wiley & Sons, Ltd.

DOI: 10.1002/fld

$$E_{Kx}=\Delta z_{i+1/2,j,Kx}+\frac{\Delta T\,\mathrm{Av}_{i,j,Kx-1/2}}{\Delta z_{i+1/2,j,Kx-1/2}}+\Delta TC_d[(u^{m-1}_{i+1/2,j,Kx})^2+((v^{m-1}_{i,j,Kx})^*)^2]^{1/2}$$

$$E'_1=(\Delta z_{i,j+1/2,1}+\zeta^{m+1/2}_{i,j})+\frac{\Delta T\,\mathrm{Av}_{i,j,3/2}}{\Delta z_{i,j+1/2,3/2}},\quad T'_1=-\frac{\Delta T\,\mathrm{Av}_{i,j,3/2}}{\Delta z_{i,j+1/2,3/2}},\quad A'_k=-\frac{\Delta T\,\mathrm{Av}_{i,j,k-1/2}}{\Delta z_{i,j+1/2,k-1/2}}$$

$$E'_k=\Delta z_{i,j+1/2,k}+\frac{\Delta T\,\mathrm{Av}_{i,j,k-1/2}}{\Delta z_{i,j+1/2,k-1/2}}+\frac{\Delta T\,\mathrm{Av}_{i,j,k+1/2}}{\Delta z_{i,j+1/2,k+1/2}}$$

$$T'_k=-\frac{\Delta T\,\mathrm{Av}_{i,j,k+1/2}}{\Delta z_{i,j+1/2,k+1/2}},\quad A'_{Ky}=-\frac{\Delta T\,\mathrm{Av}_{i,j,Ky-1/2}}{\Delta z_{i,j+1/2,Ky-1/2}}$$

$$E'_{Ky}=\Delta z_{i,j+1/2,Ky}+\frac{\Delta T\,\mathrm{Av}_{i,j,Ky-1/2}}{\Delta z_{i,j+1/2,Ky-1/2}}+\Delta TC_d[(v^{m-1}_{i,j+1/2,Ky})^2+((u^{m-1}_{i,j,Ky})^*)^2]^{1/2}$$

$F_1, F_k, F_{kx}, F'_1, F'_k, F'_{ky}$ are equal to the right sides of (B13)–(B18), respectively. Equations (B19) and (B20) are both tridiagonal systems that can be solved efficiently. After that, μ^m and γ^m can be obtained.

$Y_{i,j}, aLx_{i+1/2,j}, aLy_{i,j+1/2,}, aRx_{i+1/2,j}, aRy_{i,j+1/2}$ of AE in Appendix B.1 are calculated in AI, and their expressions are given by

$$Y_{i,j}=\sum_{k=1}^{Kx}\left[\frac{g\Delta t}{a_j\Delta\lambda}(\mu_{i+1/2,j,k}-\mu_{i-1/2,j,k})(\Delta z_{i+1/2,j,k}+\sigma_k\zeta_{i+1/2,j})\right]\Big/ Hx_{i+1/2,j}$$
$$+\sum_{k=1}^{Ky}\left[\frac{g\Delta t}{R\Delta\phi}(\gamma_{i,j+1/2,k}-\gamma_{i,j-1/2,k})(\Delta z_{i,j+1/2,k}+\sigma_k\zeta_{i,j+1/2})\right]\Big/ Hy_{i,j+1/2}$$

$$aLx_{i+1/2,j}=\frac{\sum_{k=1}^{Kx}[alx_{i+1/2,j,k}(\Delta z_{i+1/2,j,k}+\sigma_k\zeta_{i+1/2,j})]}{Hx_{i+1/2,j}}$$

$$aLy_{i,j+1/2}=\frac{\sum_{k=1}^{Ky}[aly_{i,j+1/2,k}(\Delta z_{i,j+1/2,k}+\sigma_k\zeta_{i,j+1/2})]}{Hy_{i,j+1/2}}$$

$$aRx_{i+1/2,j}=\frac{C_d\tau_{i+1/2,j}\{[u^2_{i+1/2,j,Kx}+(v^*_{i,j,Kx})^2]^{1/2}+[u^2_{i+1/2,j,Kx}+(v^*_{i,j,Kx})^2]^{-1/2}u^2_{i+1/2,j,Kx}\}}{Hx_{i+1/2,j}}$$
$$+\frac{C_d\delta^*_{i,j}[u^2_{i+1/2,j,Ky}+(v^*_{i,j,Ky})^2]^{-1/2}v^*_{i,j,Ky}u_{i+1/2,j,Ky}}{Hy_{i,j+1/2}}$$

$$aRy_{i,j+1/2}=\frac{C_d\delta_{i,j+1/2}\{[v^2_{i,j+1/2,Ky}+(u^*_{i,j,Ky})^2]^{1/2}+[v^2_{i,j+1/2,Ky}+(u^*_{i,j,Ky})^2]^{-1/2}v^2_{i,j+1/2,Ky}\}}{Hy_{i,j+1/2}}$$
$$+\frac{C_d\tau^*_{i,j}[v^2_{i,j+1/2,Kx}+(u^*_{i,j,Kx})^2]^{-1/2}u^*_{i,j,Kx}v_{i,j+1/2,Kx}}{Hx_{i+1/2,j}}$$

Copyright © 2007 John Wiley & Sons, Ltd.

DOI: 10.1002/fld

ACKNOWLEDGEMENTS

We deeply thank the two anomalous reviewers for their constructive criticism of an earlier version of the manuscript. Thanks are extended to Ms Ling Tian for her friendly help on the paper. Partial support for this research was provided by the State Ministry of Science and Technology of China through grant 2007AA09Z118, the National Basic Research Program of China through grant 2005CB422308 and the Specialized Research Fund for the Doctoral Program of Higher Education through grant 20050423007. The TOPEX/Poseidon data are provided by PODAAC of JPL.

REFERENCES

1. Leendertse JJ, Alexander RC, Liu SK. A three dimensional model for estuaries and Coastal Seas, vol. I: principles of computations. *Report R-1417-OWRR*, Rand Corporation, Santa Monica, 1973.
2. Backhaus J. A three-dimensional model for the simulation of shelf sea dynamics. *Deutsche Hydrographische Zeitschrift* 1985; **38**:165–187.
3. Casulli V, Cheng RT. Semi-implicit finite difference methods for the three dimensional shallow water flow. *International Journal for Numerical Methods in Fluids* 1992; **15**:629–648.
4. Casulli V. A semi-implicit finite difference method for the non-hydrostatic free-surface flow. *International Journal for Numerical Methods in Fluids* 1999; **30**:425–440.
5. Yuan HL, Wu CH. An implicit three-dimensional fully non-hydrostatic model for free-surface flows. *International Journal for Numerical Methods in Fluids* 2004; **46**:709–733.
6. Roache P. *Computational Fluid Dynamics*. Hermosa: Albuquerque, NM, 1982.
7. Simons TJ. Verification of numerical models of Lake Ontario, Part 1: circulation in spring and early summer. *Journal of Physical Oceanography* 1974; **4**:507–523.
8. Bennett AF, McIntosh PC. Open ocean modeling as an inverse problem: tidal theory. *Journal of Physical Oceanography* 1982; **12**:1004–1018.
9. Prevost C, Salmon R. A variational method for inverting hydrographic data. *Journal of Marine Science* 1986; **44**:1–34.
10. Sasaki Y. Some basic formalisms in numerical variational analysis. *Monthly Weather Review* 1970; **98**:875–883.
11. Thacker WC, Long RB. Fitting dynamics to data. *Journal of Geophysical Research* 1988; **93**:1227–1240.
12. Panchang VG, O'Brien JJ. On the determination of hydraulic model parameters using the adjoint state formulation. In *Modelling Marine System*, Davis AM (ed.). CRC Press: Boca Raton, FL, 1989; 6–18.
13. Smedstad OM, O'Brien JJ. Variational data assimilation and parameter estimation in an equatorial Pacific Ocean model. *Progress in Oceanography* 1991; **26**:179–241.
14. Yu LS, O'Brien JJ. Variational estimation of the wind stress drag coefficient and the oceanic eddy viscosity profile. *Journal of Physical Oceanography* 1991; **21**:709–719.
15. Yu LS, O'Brien JJ. On the initial condition parameter estimation. *Journal of Physical Oceanography* 1992; **22**:1361–1364.
16. Ghil M, Malanotte-Rizzoli P. Data assimilation in meteorology and oceanography. In *Advances in Geophysics*, vol. 33, Saltzman B (ed.). Academic Press: New York, 1991; 141–266.
17. Das SK, Lardner RW. On the estimation of parameters of hydraulic models by assimilation of periodic tidal data. *Journal of Geophysical Research* 1991; **96**:15187–15196.
18. Das SK, Lardner RW. Variational parameter estimation for a two dimensional numerical tidal model. *International Journal for Numerical Methods in Fluids* 1992; **15**:313–327.
19. Lardner RW. Optimal control of an open boundary conditions for a numerical tidal model. *Computer Methods in Applied Mechanics and Engineering* 1993; **102**:367–387.
20. Lardner RW, Das SK. Optimal estimation of eddy viscosity for a quasi-three dimensional numerical tidal and storm surge model. *International Journal for Numerical Methods in Fluids* 1994; **18**:295–312.
21. Lardner RW, Song Y. Optimal estimation of eddy viscosity and friction coefficients for a quasi-three-dimensional numerical tidal model. *Atmosphere-Ocean* 1995; **33**(3):581–611.
22. Navon Im. Practical and theoretical aspects of adjoint parameter estimation and identifiability in meteorology and oceanography. *Dynamics of Atmospheres and Oceans* 1997 **27**(3):55–79.
23. Lu J, Hsieh WW. Adjoint data assimilation in coupled atmosphere–ocean models: determining initial model parameters in a simple equatorial model. *Quarterly Journal of the Royal Meteorological Society* 1997; **123**: 2115–2139.

Copyright © 2007 John Wiley & Sons, Ltd.

DOI: 10.1002/fld

24. Lu J, Hsieh WW. Adjoint data assimilation in coupled atmosphere–ocean models: determining initial conditions in a simple equatorial model. *Journal of the Meteorological Society of Japan* 1998; **76**:737–748.
25. Lu J, Hsieh WW. On determining initial conditions and parameters in a simple coupled atmosphere–ocean model by adjoint data assimilation. *Tellus A* 1998; **50**:534–544.
26. Marotzke J, Giering R, Zhang QK, Stammer D, Hill CN, Lee T. Construction of the adjoint MIT ocean general circulation model and application to Atlantic heat transport sensitivity. *Journal of Geophysical Research* 1999; **104**:29529–29548.
27. Heemink AW, Mouthaan EEA, Roest MRT, Vollebregt EAH, Robaczewska KB, Verlaam M. Inverse 3D shallow water flow modeling of the continental shelf. *Continental Shelf Research* 2002; **22**:465–484.
28. Zhang AJ, Parker BB, Wei E. Assimilation of water level data into a coastal hydrodynamic model by an adjoint optimal technique. *Continental Shelf Research* 2002; **22**:1909–1934.
29. Zhang AJ, Wei E, Parker BB. Optimal estimation of tidal open boundary conditions using predicted tides and adjoint data assimilation technique. *Continental Shelf Research* 2003; **23**:1055–1070.
30. Peng SQ, Xie L. Effect of determining initial conditions by four-dimensional variational data assimilation on storm surge forecasting. *Ocean Modelling* 2006; **14**:1–18.
31. Lu XQ, Zhang JC. Numerical study on spatially varying bottom friction coefficient of a 2D tidal model with adjoint method. *Continental Shelf Research* 2006; **26**:1905–1923.
32. Yeh WWG. Review of parameter identification procedures in groundwater hydrology: the inverse problem. *Water Resources Research* 1986; **22**:95–108.
33. Richardson JE, Panchang VG. A modified adjoint method for inverse eddy viscosity estimation in coastal circulation models. In *Estuarine and Coastal Modeling*, Spaulding ML, Bedford K, Blumberg A, Cheng R, Swanson C (eds). Academic Press: New York, 1992; 733–745.
34. Ullman DS, Wilson RE. Model parameter estimation from data assimilation modelling: temporal and spatial variability of the bottom drag coefficient. *Journal of Geophysical Research* 1998; **103**:5531–5549.
35. Arakawa A, Lamb VR. Computational design of the basic dynamical processes of the UCLA general circulation model. In *Methods of Computational Physics*, Chang J (ed.). Academic Press: New York, 1977; 173–265.
36. Anderson DLT, Sheinbaum J, Haines K. Data assimilation in ocean models. *Reports on Progress in Physics* 1996; **59**:1209–1266.
37. Munk WH. Once again: once again-tidal friction. *Progress in Oceanography* 1997; **40**:7–35.
38. Lee JC, Jung KT. Application of eddy viscosity closure models for the M_2 tide and tidal currents in the Yellow Sea and the East China Sea. *Continental Shelf Research* 1999; **19**:445–475.
39. Egbert GD, Ray RD, Bills BG. Numerical modeling of the global semidiurnal tide in the present day and in the last glacial maximum. *Journal of Geophysical Research* 2004; **109**:C03003.
40. Lardner RW, Al-Rabeh AH, Gunay N. Optimal estimation of parameters for a two-dimensional hydro-dynamical model of the Arabian Gulf. *Journal of Geophysical Research* 1993; **98**:18229–18242.
41. He YJ, Lu XQ, Qiu ZF, Zhao JP. Shallow water tidal constituents in the Bohai Sea and the Yellow Sea from a numerical adjoint model with TOPEX/POSEIDON altimeter data. *Continental Shelf Research* 2004; **24**:1521–1529.
42. Cressman GP. An operational objective analysis system. *Monthly Weather Review* 1959; **87**:367–374.
43. Ayoub N. Estimation of boundary values in a North Atlantic circulation model using an adjoint method. *Ocean Modelling* 2006; **12**:319–347.
44. Gejadze IY, Copeland GJM, Navon IM. Open boundary control problem for Navier–Stokes equations including a free surface: data assimilation. *Computers and Mathematics with Applications* 2006; **52**:1269–1288.
45. Gejadze IY, Copeland GJM. Open boundary control problem for Navier–Stokes equations including a free surface: adjoint sensitivity analysis. *Computers and Mathematics with Applications* 2006; **52**:1243–1268.
46. Zhang JC, Zhu JG, Lu XQ. Numerical study on the bottom friction coefficient of the Bohai Sea, the Yellow Sea and the East China Sea. *Chinese Journal of Computational Physics* 2006; **23**(6):731–737.
47. Tihonov AN. Solution of incorrectly formulated problems and the regularization method. *Soviet Mathematics Doklady* 1963; **4**:1035–1038.
48. Tihonov AN. Regularization of incorrectly posed problems. *Soviet Mathematics Doklady* 1963; **4**:1624–1627.

Copyright © 2007 John Wiley & Sons, Ltd.

DOI: 10.1002/fld